https://doi.org/10.5194/egusphere-2025-1182
Preprint. Discussion started: 25 March 2025

Quantitative reconstruction of deglacial bottom-water nitrate in marginal Pacific seas using the pore density of denitrifying benthic foraminifera

Anjaly Govindankutty Menon[1*], Aaron L. Bieler[2, 3], Hanna Firrincieli[1], Rachel Alcorn[4], Niko Lahajnar[1, 6] Catherine V. Davis[4], Ralf Schiebel[2], Dirk Nürnberg[5], Gerhard Schmiedl[1, 6], Nicolaas Glock[1]

[1]*Department of Earth System Sciences, Institute for Geology, Universität Hamburg, Bundesstrasse 55, D - 20146 Hamburg, Germany*

[2]*Climate Geochemistry Department Max Planck Institute for Chemistry, Hahn-Meitner-Weg 1, D - 55128 Mainz, Germany*

[3]*Department of Earth and Planetary Sciences, ETH Zürich, Sonneggstrasse 5, 8092 Zürich, Switzerland*

[4]*Department of Marine, Earth, and Atmospheric Sciences, North Carolina State University, 2800 Faucette Dr, Raleigh, NC, 27607, United States*

[5]*GEOMAR Helmholtz Centre for Ocean Research Kiel, Wischhofstr. 1-3, Geb. 8c, Raum 106, D-24148 Kiel, Germany*

[6]*Center for Earth System Research and Sustainability, Institute for Geology, Universität Hamburg, Bundesstrasse 55, D-20146 Hamburg, Germany*

**Corresponding author: anjaly.govindankutty.menon@uni-hamburg.de*

https://doi.org/10.5194/egusphere-2025-1182
Preprint. Discussion started: 25 March 2025

Abstract

Quantifying past ocean nitrate concentrations is crucial for understanding the global nitrogen cycle. Here, we reconstruct deglacial bottom-water nitrate concentrations ($[NO_3^-]_{BW}$) reconstruction in the oxygen-deficient zones of the Sea of Okhotsk, the Gulf of California, the Mexican Margin, and the Gulf of Guayaquil. Using the pore density of denitrifying benthic foraminifera as a nitrate proxy, differences in $[NO_3^-]_{BW}$ are observed at the study sites spanning the Last Glacial Maximum to the Holocene. Changes in water-column denitrification, water-mass ventilation, primary productivity, and sea surface temperatures may account for nitrate differences at the study sites. The $[NO_3^-]_{BW}$ in the Sea of Okhotsk, the Gulf of California, and the Gulf of Guayaquil are influenced by the intermediate water masses while, the $[NO_3^-]_{BW}$ at the Mexican Margin is likely influenced by deglacial changes in the Pacific Deep Water. The comparison of past and present $[NO_3^-]$ shows that the modern Gulf of Guayaquil and the Gulf of California currently have stronger oxygen-deficient zones with higher denitrification than during the Last Glacial Maximum. In contrast, the modern Mexican Margin and the Sea of Okhotsk may have higher oxygen, indicated by low modern denitrification than during the Last Glacial Maximum.

https://doi.org/10.5194/egusphere-2025-1182
Preprint. Discussion started: 25 March 2025

1. Introduction

The marine nitrogen cycle is a complex web of microbially mediated processes controlling the inventory and distribution of bioavailable nitrogen in marine environments (Casciotti, 2016). Biological nitrogen fixation by nitrogen-fixing diazotrophs (e.g., cyanobacteria) in the surface layer is the main source of bioavailable nitrogen in the ocean, and denitrification and anammox, are the main fixed nitrogen loss processes (Lam and Kuypers, 2011), both of which occur under low-oxygen conditions. The primary form of bioavailable nitrogen in the ocean is nitrate (NO_3^-), (Casciotti 2016), which is a limiting nutrient throughout the tropical and subtropical oceans (Moore et al., 2013).

Oxygen-deficient zones (ODZs) are regions of very low oxygen (O_2) where the O_2 concentration is less than 22 µmol/kg, usually within depths of 100 – 1,200 m (Levin, 2003; 2018). Oxygen plays a key role in the marine nitrogen cycle (Keeling et al., 2010) because some microbial processes require oxygen while others are inhibited by it (Voss et al., 2013). For example, denitrification (reduction of nitrate to dinitrogen gas) in the ocean occurs only in suboxic (oxygen <5µmol/kg) conditions (Codispoti et al., 2001; Levin, 2018). On a global scale, ~30-50% of fixed nitrogen loss in the world's oceans occurs in ODZs (Gruber, 2008), either through denitrification or anammox (Devol et al., 2006; Lam and Kuypers, 2011; Evans et al., 2023). Benthic denitrification plays an important role in shaping global nitrogen fixation, and net primary production (Somes et al., 2017; Li et al., 2024). ODZs cover only 1% of the world's seafloor (Codispoti et al., 2001), however, 10% of the global benthic denitrification occurs in these regions (Bohlen et al., 2012). Observations and climate model simulations predicted the expansion of ODZs (Stramma et al., 2008, 2010; Schmidtko et al., 2017; Oschlies, 2021) to continue at least until the year of 2100. However, the evolution of ODZs on timescales of hundreds to thousands of years remains uncertain (Yamamoto et al., 2015; Takano et al., 2018, Fu et al., 2018; Frölicher et al., 2020). Considering the role of ODZs in modulating the marine nitrogen cycle, it is of key scientific interest to understand how nitrogen cycling works in these ecosystems and the potential factors that influence the nitrogen cycle.

The stable isotope signature of nitrogen in the sedimentary organic matter ($\delta^{15}N_{bulk}$) is an established proxy for water-column denitrification and for understanding changes associated with nutrient utilization (Thunell et al., 2004; Robinson et al., 2009; Martinez and Robinson, 2010; Dubois et al., 2011, 2014; Tesdal et al., 2013; Wang et al., 2019; Riechelson et al., 2024). An

https://doi.org/10.5194/egusphere-2025-1182
Preprint. Discussion started: 25 March 2025

increase (or decrease) in nutrient availability in relation to nutrient demand results in an increase (or decrease) in $\delta^{15}N$ values (Wada and Hattori, 1978; Montoya, 1990). When oxygen supply in the ocean is reduced, either due to global warming or increased availability of organic matter for remineralization, sedimentary $\delta^{15}N$ increases alongside intensified water column denitrification (Wang et al., 2019). Therefore, $\delta^{15}N_{bulk}$ can be an important tool for reconstructing past changes in denitrification in the ODZs. During the last glacial period, $\delta^{15}N_{bulk}$ measurements suggest that denitrification rates within ODZs increased from the Last Glacial Maximum (LGM) to the Holocene (Robinson et al., 2009, Martinez and Robinson, 2010). The $\delta^{15}N_{bulk}$ records from the whole sediment can be subject to various processes/or sources which can complicate their interpretation. For example, diagenetic alteration during sinking in the water column and burial in the sediment (Altabet and Francois, 1994; Lourey et al., 2003), as well as terrestrial or shelf sources of organic and inorganic nitrogen (Schubert & Calvert, 2001; Kienast et al., 2005; Meckler et al., 2011), and remotely advected water masses with different $\delta^{15}N$ values (for e.g., Southern Californian margin; Liu and Kaplan, 1989), could influence the $\delta^{15}N$ signatures in sediments. Nevertheless, Tesdal et al. (2013) proposed that $\delta^{15}N_{bulk}$ can be a reliable indicator for individual locations reflecting the oceanographic conditions of the surrounding environments.

Foraminifera are unicellular eukaryotes that are abundant in marine environments (Goldstein, 1999), and can be either planktic or benthic. The nitrogen isotopes of organic matter bound and protected within the calcite shell of planktic foraminifera ($\delta^{15}N_{FB}$) are less subjected to diagenesis or sedimentary contamination and can be used to understand major nitrogen transformations occurring in the ocean (Ren et al., 2012; Studer et al., 2021). Recent studies based on $\delta^{15}N_{FB}$ have shown that water column denitrification decreased and ODZs contracted during warmer-than-present periods of the Cenozoic (Auderset et al., 2022; Hess et al., 2023; Moretti et al., 2024). Another study based on $\delta^{15}N_{FB}$ (Studer et al., 2021) suggests that water column denitrification was at its peak during the deglaciation but was comparable during the LGM and the Holocene in the Eastern Equatorial Pacific. In contrast, Riechelson et al. (2024) used $\delta^{15}N_{bulk}$ and hypothesized that the decrease in $\delta^{15}N_{bulk}$ values over the Holocene is related to a decrease in Southern Ocean nutrient utilization and not due to a decrease in denitrification. Other studies (Ganeshram et al., 2002; Deutsch et al., 2004; Eugster et al., 2013) have shown that reactive nitrogen inventories were elevated during glacial periods, largely due to reduced denitrification in the water column and sediments.

https://doi.org/10.5194/egusphere-2025-1182
Preprint. Discussion started: 25 March 2025

Benthic foraminifera are responsible for a large fraction of benthic denitrification in ODZs (Piña-Ochoa et al., 2010a; 2010b; Glock et al., 2013; Dale et al., 2016). Some species for example; *Bolivina spissa* which are abundant in ODZs in and around the Pacific Ocean (Glock et al., 2011; Fontanier et al., 2014) can use NO_3^- as an electron acceptor (see Fig. 1 (a)) and thus can denitrify (Risgaard-Petersen 2006; Piña-Ochoa et al., 2010a; 2010b).

A study by Glock et al. (2019) proposed for some denitrifying foraminifera, denitrification is their preferred respiration pathway. The uptake of NO_3^- by these foraminifera is likely through pores in the test (see Fig. 1 (a)). Nitrate is completely denitrified to dinitrogen gas (N_2) partly by the foraminifera themselves (Risgaard-Petersen 2006; Woehle and Roy et al., 2018; Orsi et al., 2020; Gomaa et al., 2021), and partly supported by prokaryotic endobionts (Bernhard et al., 2012a, Woehle and Roy et al., 2022).

To date, benthic foraminifera are the only eukaryote holobiont known to perform complete heterotrophic denitrification (Risgaard-Petersen 2006; Kamp et al., 2015). Every *Bolivina* species tested so far (including *Bolivina seminuda*), can denitrify (Piña-Ochoa et al., 2010a; Bernhard et al., 2012b), suggesting that denitrification is a common survival strategy of Bolivinidae under oxygen-depleted conditions (Glock et al., 2019). In low-oxygen environments, such as the ODZs off Peru, Costa Rica, and the hypoxic Sagami Bay, *B. spissa* increase their pore density with decreasing ambient NO_3^- availability. Thus, their pore density is significantly, linearly correlated with bottom water nitrate concentrations (see Fig. 1 (b)) in their habitat (Glock et al., 2011; Govindankutty Menon et al., 2023). Therefore, the pore density of several Bolivina species such as *B. spissa*, and *B. subadvena* is a promising empirical proxy for paleo-NO_3^- reconstruction (Glock et al., 2018; Govindankutty Menon et al., 2023).

https://doi.org/10.5194/egusphere-2025-1182
Preprint. Discussion started: 25 March 2025

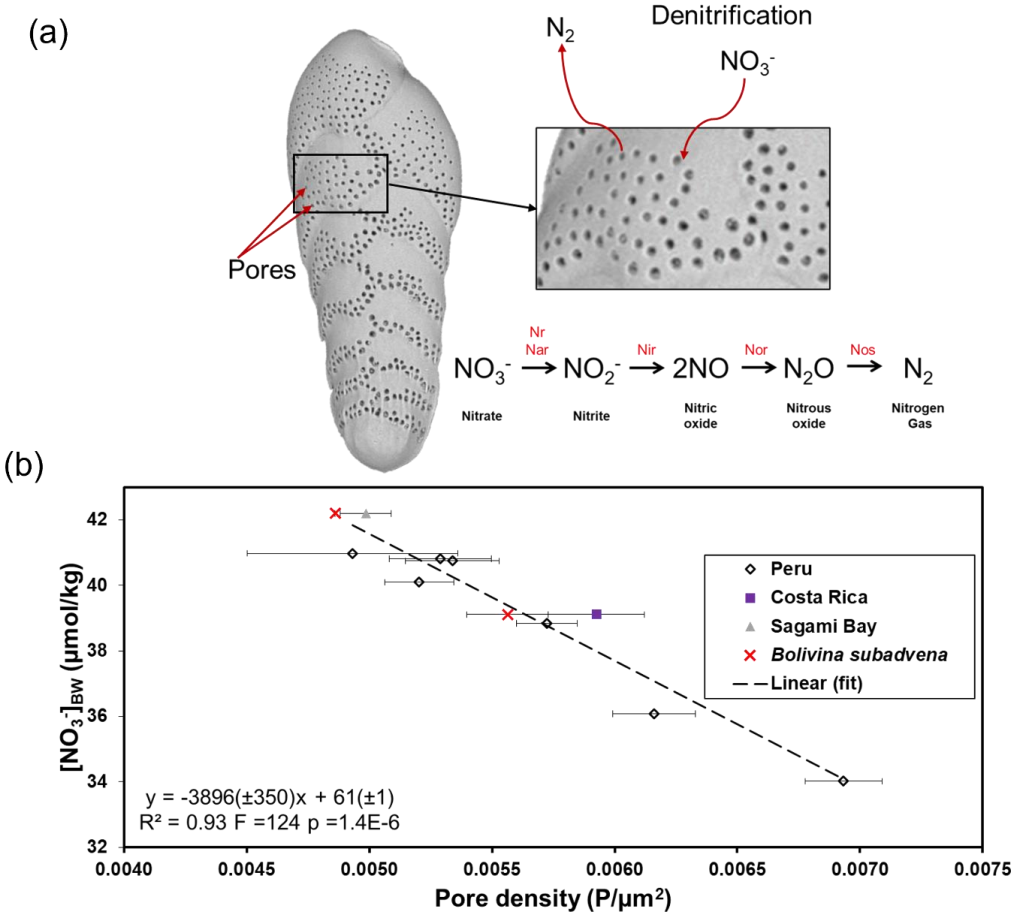

Figure 1: The (a) schematic view of nitrate (NO_3^-) uptake, and the excretion of nitrogen gas (N_2) by the benthic foraminifera *Bolivina spissa*. The step-wise denitrification pathway from NO_3^- to N_2 involving enzymes such as nitrate reductase (Nr Nar), nitrite reductase (Nir), nitric-oxide reductase (Nor), and nitrous oxide reductase (Nos) is also shown. (b) Correlation between pore density of *Bolivina spissa* from Peru, off Costa Rica, Sagami Bay, and *Bolivina subadvena* with bottom-water nitrate $[NO_3^-]_{BW}$ from Govindankutty Menon et al. (2023). The error bars are 1 standard error of the mean.

In this study, we use the pore density (number of pores per unit area) of *B. spissa* and *B. subadvena* as a NO_3^- proxy (Govindankutty Menon et al., 2023) to reconstruct $[NO_3^-]_{BW}$ in intermediate water depths of the Sea of Okhotsk, the Gulf of California, the Gulf of Guayaquil, and in the Pacific Deep Water (PDW) depths of the Mexican Margin (Fig. 2 and 3). The $[NO_3^-]_{BW}$ calibration using

https://doi.org/10.5194/egusphere-2025-1182
Preprint. Discussion started: 25 March 2025

the pore density of *B. spissa* and *B. subadvena* (see Fig. 1 (b)) developed in Govindankutty Menon et al. (2023) is applied in the current study. Combining a proxy for bottom-water nitrate $[NO_3^-]_{BW}$ (pore density of denitrifying foraminifera) and a proxy for N-cycle processes in the water column ($\delta^{15}N_{bulk}$) might facilitate a more comprehensive understanding of past N-cycling in different zones of the water column. Here, we try to understand whether 1) there are differences in reconstructed $[NO_3^-]_{BW}$ between glacial and deglacial periods in the four studied sites, 2) the reconstructed $[NO_3^-]_{BW}$ records are in agreement with $\delta^{15}N_{bulk}$ data, and 3) there was more or less NO_3^- in the past than today.

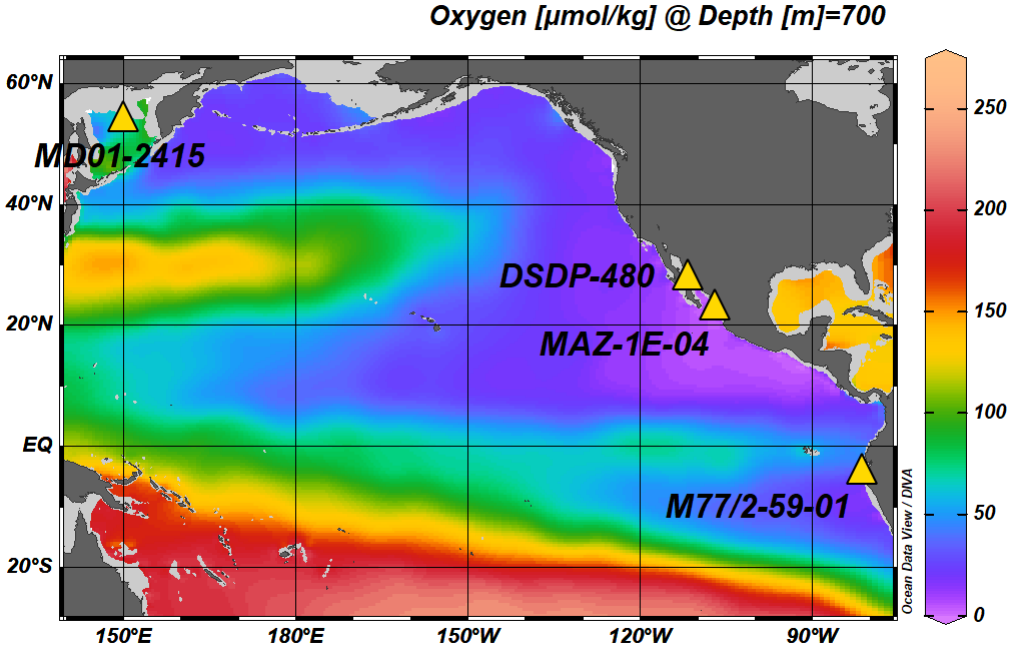

Figure 2. Location of sediment cores used in the current study and mean annual oxygen concentrations at 700 m depth (Garcia et al., 2019). Sediment cores are indicated by yellow triangles: Sea of Okhotsk (core MD01-2415; water depth: 822 m), Gulf of California (DSDP Site-480; water depth: 747 m), Mexican Margin (core MAZ-1E-04; water depth: 1463 m), and Gulf of Guayaquil (core M77/2-59-01; water depth: 997 m). Map created with Ocean Data View (Schlitzer, R., 2023).

https://doi.org/10.5194/egusphere-2025-1182
Preprint. Discussion started: 25 March 2025

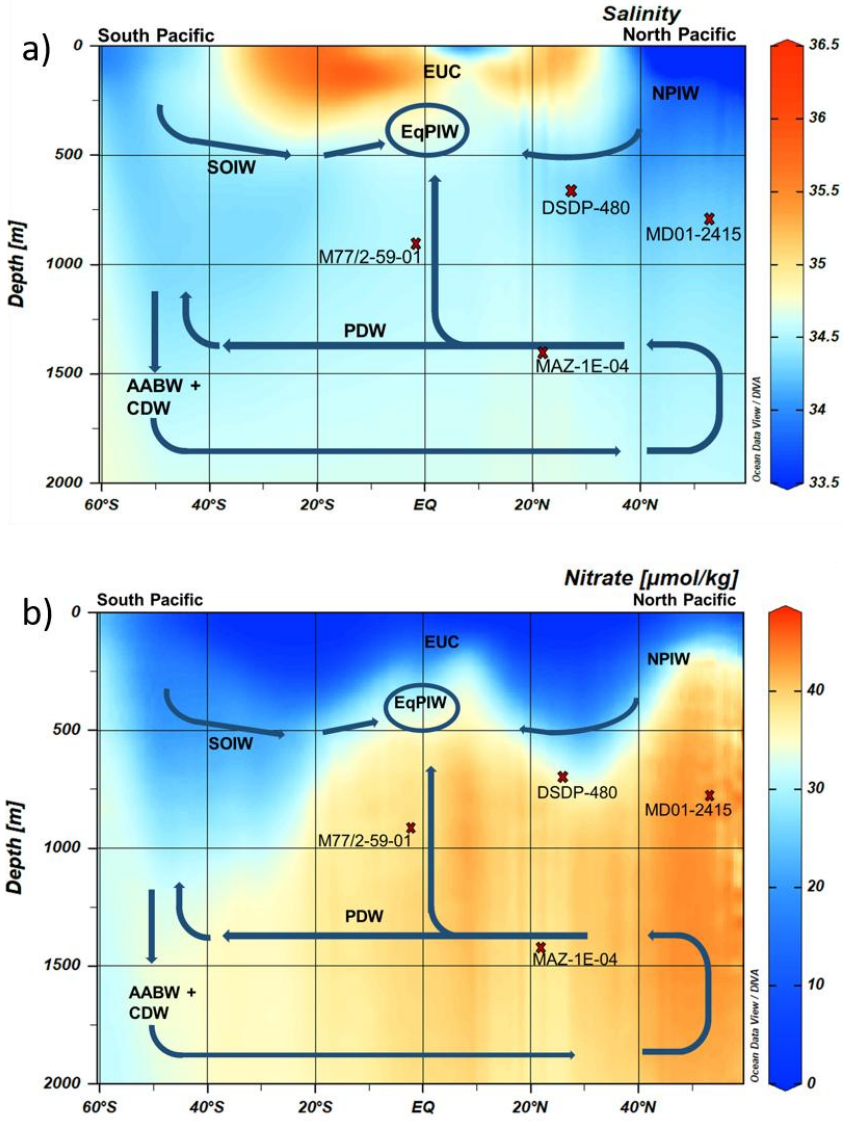

Figure 3. Modern a) salinity and b) nitrate distribution along a N-S transect across the Pacific (Garcia et al., 2019) with major subsurface and deep-water masses (blue arrows) and formation areas of North Pacific Intermediate Water (NPIW) and Southern Ocean Intermediate Water (SOIW) are included. Sediment cores used for $[NO_3^-]_{BW}$ reconstruction are shown (red crosses) projected to the N-S hydrographic transect. Equatorial Pacific Intermediate Water (EqPIW), Equatorial Undercurrent (EUC), NPIW, SOIW, Pacific Deep Water (PDW), Antarctic Bottom Water (AABW), and Circumpolar Deep Water (CDW). Profiles generated by Ocean Data View (Schlitzer, R., 2023) using the data from World Ocean Atlas 2018 (Garcia et al., 2019).

https://doi.org/10.5194/egusphere-2025-1182
Preprint. Discussion started: 25 March 2025

2. Materials and methods

2.1 Study area and sampling of sediment cores. We used downcore samples from the Eastern Tropical South Pacific, ETSP (Gulf of Guayaquil (M77/2-59-01), Eastern Tropical North Pacific the ETNP (Mexican Margin, MAZ-1E-04), the Gulf of California (Guaymas Basin, DSDP-64-480), and the Sea of Okhotsk (MD01-2415), over the last ~20,000 years (Fig. 3). The Gulf of Guayaquil sediment core M77/2-59-01 (03°57.01′ S, 81°19.23′ W, recovery 13.59 m) was collected from the northern edge of the ODZ at a water depth of 997 m during the RV Meteor cruise M77/2 in 2008 (Mollier-Vogel et al., 2013, 2019; Nürnberg et al., 2015). The piston core MAZ-1E-04, Mexican Margin (22.9°N, 106.91°W) was collected on board the RV El Puma at a water depth of 1463 m. The CALYPSO giant piston core MD01-2415 (53°57.09' N, 149°57.52' E, recovery 46.23 m) was recovered from the northern slope of the Sea of Okhotsk at 822 m water depth during the WEPAMA cruise MD122 of the R/V Marion Dufresne (Holbourn et al., 2002; Nürnberg & Tiedemann, 2004). The Deep-Sea Drilling Project core DSDP- 480 (27°54' N, 111°39' W) from the Gulf of California was retrieved at a water depth of 747 m close to the Guaymas Basin.

2.2 Sampling of foraminiferal specimens for the quantitative nitrate record. A total of 1541 fossil specimens of *B. spissa* (number of specimens, n =1268) and *B. subadvena* (n = 273) were used for the $[NO_3^-]_{BW}$ reconstructions across the four sites. A total of 37 sample depths (n = 669) from the Gulf of Guayaquil (M77/2-059-1), 23 sample depths (n = 455) from the Mexican Margin (MAZ-1E-04), 16 sample depths (n = 273) from the Gulf of California (DSDP-480), 11 sample depths (n= 144) from the Sea of Okhotsk (MD01-2415) were utilized. Porosity measurements were made on 6–20 well-preserved specimens of *B. spissa* and *B. subadvena* in each sample. The sediment samples were washed and wet-sieved through a 63 µm mesh sieve. The residues were dried in an oven at 38-50°C. The samples were sieved into the grain-size fractions of 63-125, >125-250, >250-315, >315-355, >355-400, and >400 µm. Specimens of *B. spissa*, and *B. subadvena* were picked from the 125-250 µm fraction.

2.3 Automated image analysis. All specimens of *B. spissa* and *B. subadvena* were imaged using a Scanning Electron Microscope (Hitachi Tabletop SEM TM4000 series) at Hamburg University, Germany with an accelerating voltage of 15 kV using a back-scattered electron (BSE) detector. The specimens were not sputter-coated to allow for future geochemical analyses. For porosity

https://doi.org/10.5194/egusphere-2025-1182
Preprint. Discussion started: 25 March 2025

measurements, the total area on the first (oldest) ten chambers (equivalent to an area of 50,000 to 70,000 µm^2) was measured using the ZEN 3.4 blue edition software. Size normalization was done to minimize the impact of ontogenetic effects on the pore density. The pore parameters such as the pore density (PD), mean pore size, and porosity were determined with the automated image analyzing software Amira^{TM} 3D pro using a previously trained deep-learning algorithm. The deep learning algorithm that was used for this study is included in the Amira software package. The deep learning algorithm was initially trained with manually segmented pores on 52 images of *B. spissa* and 60 images of *B. subadvena*. Only those specimens that had a total area equivalent to at least 50,000 µm^2 were used for the automated analysis. Data from smaller specimens that did not fit within the minimal total area were discarded. The detailed methodology of the porosity measurements and trained deep-learning algorithm is described in Govindankutty Menon et al. (2023).

Following the image analysis, pore density data of benthic foraminifera from the four ODZs were used for the quantitative reconstruction of $[NO_3^-]_{BW}$ (Fig. 6). We distinguished five different time intervals, including the Last Glacial Maximum (LGM; 22–17 ka BP), Heinrich Stadial 1 (H1; 17–15 ka BP), Bølling - Allerød (BA; 14.7-12. 9 ka BP), Younger Dryas (YD; 12.9–11.7 ka BP), Early Holocene (EH; 11.7–8.2 ka BP) and Middle to Late Holocene (MLH; 8–0 ka BP) to describe the $[NO_3^-]_{BW}$ in the East Pacific and the Sea of Okhotsk (Fig. 6). The $[NO_3^-]_{BW}$ from all cores were calculated using the calibration equation;

$$[NO_3^-]_{BW} = -3896\ (\pm 350)\ PD + 61(\pm 1) \quad (1)$$

where PD is the pore density of benthic foraminifera (Govindankutty Menon et al., 2023).

The standard error of the mean (SEM) for one sample was calculated using the equation;

$$SEM_{[NO_3^-]_{BW}} = \frac{SD_{[NO_3^-]_{BW}}}{\sqrt{n}} \quad (2)$$

where n is the number of specimens analyzed in each sample and SD is 1 standard deviation of mean reconstructed $[NO_3^-]_{BW}$.

$$SD_{[NO_3^-]_{BW}} = \sqrt{(350\ X\ PD)^2 + (-3896\ X\ SD_{PD})^2 + (1)^2} \quad (3)$$

A complete error propagation was done for the calculation of the errors of the reconstructed $[NO_3^-]_{BW}$ including both the uncertainty of the mean PD within the samples and the uncertainties of the calibration function. The reconstructed $[NO_3^-]_{BW}$ and the calculated SEM and SD of each sample are shown in the Supplementary files.

https://doi.org/10.5194/egusphere-2025-1182
Preprint. Discussion started: 25 March 2025

2.4 Optimization of age models

We here present updated chronostratigraphies of cores studied, mainly based on accelerator mass spectrometry (AMS) radiocarbon (^{14}C) datings.

Sea of Okhotsk: We used the age-tie points and ^{14}C-ages published by Bubenshchikova et al. (2015); based on Nürnberg and Tiedemann, (2004) for the age model of core MD01-2415. The accelerator mass spectrometry (AMS) ^{14}C dates were incorporated in between the age-tie points to minimize the age uncertainty. For the current study, the age-depth model was updated using Marine20 (Heaton et al., 2020) within the Bchron package (Haslett & Parnell, 2008) in RStudio (RStudio Team, 2023) with a local DeltaR of 546 years from the Davydov Cape (Kuzmin et al., 2007).

Gulf of California: We used raw ^{14}C ages of planktic foraminifera from Keigwin and Jones **(**1990) for updating the age-depth model for DSDP Site 480**.** Radiocarbon age calibration was done using Marine20 with a local DeltaR of 301 years from the Guaymas Basin (Goodfriend and Flessa, 1997). The Bchron package was used for determining the age-depth model and calibrating the age.

Mexican Margin: The age model for core MAZ-1E-04 has been entirely built in the framework of the current study. We used planktic foraminifera *Globigerinoides ruber, Globigerinoides bulloides, Trilobatus sacculifer* for the AMS ^{14}C dating. Approximately 200 tests of these species were selected from the 125-250 µm fraction. The radiocarbon measurements of planktic foraminifera were carried out at the Alfred-Wegener-Institute (AWI) in Bremerhaven, Germany using the MICADAS system and at the National Ocean Sciences Accelerator Mass Spectrometry Facility, USA. We applied a manual continuous Marine Reservoir Age (MRA) correction using the MRAs from the closest available location to the core MAZ-1E-04 from the published literature (Butzin et al., 2020). Then the corresponding MRAs were subtracted from the raw ^{14}C ages of planktic foraminifers to achieve the atmospheric ^{14}C age. Radiocarbon age calibration was done using Intcal20 (Reimer et al., 2020) in the Bchron package in RStudio.

Gulf of Guayaquil: The published age model of core M77/2-59-01 (Mollier-Vogel et al., 2019) is based on ten AMS ^{14}C ages measured using planktic foraminifera species *Neogloboquadrina dutertrei* at the Leibniz Laboratory at Kiel University, Germany. For the current study, the age-

https://doi.org/10.5194/egusphere-2025-1182
Preprint. Discussion started: 25 March 2025

depth model was updated using Marine20 in the Bchron package (Haslett & Parnell, 2008) in RStudio with a DeltaR of 200 ± 50 years (Mollier-Vogel et al., 2013).

All information used for developing and updating the age models are shown in the Supplementary files.

2.5 Sedimentary nitrogen isotope ($\delta^{15}N_{bulk}$) measurements. We have measured sedimentary nitrogen isotope ($\delta^{15}N_{bulk}$) rather than $\delta^{15}N_{FB}$ from cores taken from the Sea of Okhotsk, and Gulf of California, because the low abundances of foraminifera were utilized for other analysis. The analysis of bulk sediments allows for high-resolution records. Prior to the $\delta^{15}N_{bulk}$ measurements, the Total Nitrogen (TN%) content of 20 sediment samples from the Sea of Okhotsk and 54 samples from the Gulf of California were measured at the Institute for Geology, Hamburg University, Germany using a flash combustion method with a Eurovector EA-3000 analyzer. The $\delta^{15}N_{bulk}$ measurements for both the Sea of Okhotsk and the Gulf of California were accomplished at the Max Planck Institute for Chemistry (Mainz), Germany using a DELTA V ADVANTAGE Isotope Ratio Mass Spectrometer (IRMS) equipped with a FLASH 2000 Organic Elemental Analyzer. The results were expressed in standard δ-notation (equation 4). The standard deviation (±SD) of all individual analysis runs based on a certified international reference standard (USGS65) and internal laboratory standards (L-Phenylalanine and L-Glutamic acid) referenced to certified international reference standards was < 0.3‰. The $\delta^{15}N_{bulk}$ data for the Sea of Okhotsk and the Gulf of California are shown in Supplementary Table ST1.

$$\delta^{15}N\ (‰) = [(^{15}N{:}^{14}N_{sample} / ^{15}N{:}^{14}N_{air}) - 1] \times 1{,}000 \qquad (4)$$

For the Gulf of Guayaquil core M77/2-59-01, the $\delta^{15}N_{bulk}$ data published by Mollier-Vogel et al. (2019) was used. Their measurements were done on ~ 5–50 mg of homogenized and freeze-dried bulk sediments using a Carlo-Erba CN analyzer 2500 interfaced directly to a Micromass-Isoprime mass spectrometer at Bordeaux University. Results are expressed in standard δ-notation (equation 4) relative to atmospheric dinitrogen gas (N_2).

2.6 Nitrate offset to present conditions. The reconstructed $[NO_3^-]_{BW}$ from each location is subtracted from the modern $[NO_3^-]$ present at the respective locations from similar water depths the cores were retrieved from. This provided the $[NO_3^-]$ offset which is the difference ($\Delta[NO_3^-]$ (μM)) between the modern $[NO_3^-]$ and the past reconstructed $[NO_3^-]_{BW}$. The modern $[NO_3^-]$ for

https://doi.org/10.5194/egusphere-2025-1182
Preprint. Discussion started: 25 March 2025

each location was taken from World Ocean Atlas 2018 (Garcia et al., 2019). The details are given in Table 1.

Table 1. Site location information of modern [NO_3^-] taken for the nitrate offset from World Ocean Atlas 2018.

Locations	Latitude	Longitude	Water depth (m)	Station ID	[NO_3^-] (µmol/kg)
Gulf of Guayaquil, (M77/2-59-01)	3.5° S	81.5°W	1050	21457 (B)	42.5
Mexican Margin, (MAZ-1E-04)	21.5°N	106.5°W	1450	27910 (B)	42.75
Sea of Okhotsk, (MDO1-2415)	53.5°N	149.5°E	850	33729 (B)	43.4
Gulf of California, (DSDP, 480)	27.5°N	111.5°W	750	29197 (B)	35.3

2.7 Organic carbon accumulation rates. Organic carbon accumulation rates for cores from the Sea of Okhotsk, the Gulf of California, and the Gulf of Guayaquil were calculated using the sedimentary total organic carbon weight percentage, sediment dry bulk density, and sedimentation rates (equation 5).

$$\text{TOC Accumulation rate} = \text{Sedimentation rate} \times \text{sediment dry bulk density} \times \text{TOC (wt\%)} \quad (5)$$

The sedimentation rates were calculated from the age-depth model that has been updated within this study. The total organic carbon content and dry bulk densities were taken from Bubenshchikova et al. (2015) for the Sea of Okhotsk, Leclaire and Kerry (1982) for the Gulf of California, and Mollier-Vogel et al. (2019) for the Gulf of Guayaquil. Organic carbon data was not available for core MAZ-1E-04 from the Mexican Margin. High-resolution dry bulk densities were not available for DSDP Site 480 from the Gulf of California. For this core, dry bulk densities have been calculated using the wet dry bulk density and porosity of the sediment shown in figure

https://doi.org/10.5194/egusphere-2025-1182
Preprint. Discussion started: 25 March 2025

24 of Curray et al. (1982). Since the resulting dry bulk data resolution for this core was very sparse for each depth in the core, the dry bulk density of the closest data point was used. There was a large data gap between the 2 m and 9 m sediment depth, with a considerable jump in the dry bulk density between these two sampling depths. Thus, between these two data points, dry bulk densities were linearly interpolated. The data for the organic carbon accumulation rate is given in the Supplementary files.

2.8 Statistical analysis. The statistical analyses presented in this paper were carried out using RStudio. The t-test was used to test for the significant difference between datasets of unequal sample sizes after carrying out an initial variance test. The confidence interval of 95% ($p < 0.05$) was set for the significance test.

3. Results

We reconstructed deglacial $[NO_3^-]_{BW}$ using downcore sediment samples from the Sea of Okhotsk (MD01-2415), the Gulf of California (DSDP- 480), the Mexican Margin (MAZ-1E-04), and the Gulf of Guayaquil (M77/2-59-01). The reconstructed $[NO_3^-]_{BW}$ was compared to $\delta^{15}N_{bulk}$ records of all cores (Fig. 4). All data records presented cover the time period starting from the Last Glacial Maximum, except for the core from the Sea of Okhotsk, which covers the late deglacial to the Holocene.

3.1 Sea of Okhotsk (MD01-2415). The Sea of Okhotsk core MD01-2415 covers the Younger Dryas, (YD, 12.8 ka BP) until the Middle to Late Holocene (MLH, 4.9 ka BP). The reconstructed $[NO_3^-]_{BW}$ values range from 32.8 µmol/kg to 44.1 µmol/kg (Fig. 4a). A gradual increase in $[NO_3^-]_{BW}$ is observed from the Younger Dryas to the Middle to Late Holocene. At the beginning of the Younger Dryas at 12.8 ka BP, $[NO_3^-]_{BW}$ were relatively high and then decreased to a minimum value of 32.8 µmol/kg at 12.4 ka BP. Since then, $[NO_3^-]_{BW}$ steadily increased until the Middle to Late Holocene (MLH, 44.1 µmol/kg) (Fig. 4a). The $[NO_3^-]_{BW}$ during the Middle to Late Holocene (mean = 41.2 µmol/kg) is significantly (t-test, $p = 0.023$) higher than during the Younger Dryas (mean = 36.7 µmol/kg). The sedimentary $\delta^{15}N_{bulk}$ record covers the interval from the Late Heinrich Stadial 1 (H1, 15.4 ka BP) to the Middle Holocene (6.1 ka BP). The $\delta^{15}N_{bulk}$ values were relatively high ranging from 7.1‰ to 9.4‰ with an average of 8.7‰. The $\delta^{15}N_{bulk}$ values increased steadily from the Late Heinrich Stadial 1 (15.4 ka BP) to the Early Holocene (EH, 10 ka BP) with

https://doi.org/10.5194/egusphere-2025-1182
Preprint. Discussion started: 25 March 2025

higher values centered between the Late Younger Dryas (11.9 ka BP) and the beginning of the Early Holocene. Since then, the $\delta^{15}N_{bulk}$ values decreased until the Middle to Late Holocene.

3.2 Gulf of California (DSDP-480). The analyzed sections of DSDP Site 480 covered the Last Glacial Maximum (22 ka BP) until the Early Holocene (10.8 ka BP). The reconstructed $[NO_3^-]_{BW}$ ranged from 41.4 µmol/kg to 49.1 µmol/kg. The highest $[NO_3^-]_{BW}$ of 49.1 µmol/kg occurred during the Last Glacial Maximum (18.2 ka BP). The data points from the Early Holocene (11.6-10.8 ka BP) were the only Holocene data from this core providing the lowest $[NO_3^-]_{BW}$ estimate of 42.1 µmol/kg during the Early Holocene (10.8 ka BP) (Fig. 4b). A distinct difference in $[NO_3^-]_{BW}$ between the glacial period (mean = 46.1 µmol/kg) and the Early Holocene (42.7 µmol/kg) was observed with $[NO_3^-]_{BW}$ found to be substantially higher during the glacial period (t-test, p = 0.0067) (Fig. 4b). Accordingly, the $[NO_3^-]_{BW}$ followed a decreasing pattern from the glacial period to the Early Holocene. The $\delta^{15}N_{bulk}$ values varied between 6.4‰ and 13‰ with an average of 10.2‰ (Fig. 4b). The $\delta^{15}N_{bulk}$ values from the Guaymas Basin were similar to the $\delta^{15}N_{bulk}$ values (average 9.6‰) of Pride (1997) and Altabet et al. (1999). During the last glacial period, the $\delta^{15}N_{bulk}$ values were low ranging from 8.5‰ to 9‰. At the onset of the deglaciation, the $\delta^{15}N_{bulk}$ values increased by more than 2‰ with large-scale changes reaching a maximum of 13‰ during the Younger Dryas. Afterward, we observed a gradual decline in $\delta^{15}N_{bulk}$ values throughout the Middle to Late Holocene (mean 10.7‰) and this pattern continued to the present.

3.3 Mexican Margin (MAZ-1E-04). This core MAZ-1E-04 covered the Last Glacial Maximum (20.5 ka BP) until the Early Holocene (10.47 ka BP). The $[NO_3^-]_{BW}$ values range from 37.7 µmol/kg to 43.5 µmol/kg. We observed the highest $[NO_3^-]_{BW}$ during the Younger Dryas. From the beginning to the end of the Last Glacial Maximum, $[NO_3^-]_{BW}$ followed a decreasing trend (Fig. 4c). The $[NO_3^-]_{BW}$ levels continued to steadily decrease until Heinrich Stadial 1 and consistently stayed low throughout this period. There was a strong change in $[NO_3^-]_{BW}$ from the end of Heinrich Stadial 1 to the end of Younger Dryas (Fig. 4c). We observed a peak in $[NO_3^-]_{BW}$ from the beginning of Bølling-Allerød, BA (14.29 ka BP) and it continued throughout the Younger Dryas (Fig. 4c). Afterwards, $[NO_3^-]_{BW}$ declined during the Early Holocene. The $\delta^{15}N_{bulk}$ values taken from Alcorn et al. (2025) followed an increasing trend from the glacial towards the deglacial period (Fig.4c).

3.4 Gulf of Guayaquil (M77/2-59-01). This core covered the Last Glacial Maximum (18 ka BP) until the Middle to Late Holocene (0.18 ka BP). The reconstructed $[NO_3^-]_{BW}$ values range from

https://doi.org/10.5194/egusphere-2025-1182
Preprint. Discussion started: 25 March 2025

40.5 µmol/kg to 46.5 µmol/kg. The highest $[NO_3^-]_{BW}$ occurred during the Last Glacial Maximum (Fig. 4d). The reconstructed $[NO_3^-]_{BW}$ levels during the Last Glacial Maximum (mean = 45.6 µmol/kg) were slightly higher than during the Middle to Late Holocene (mean = 44.9 µmol/kg) (t-test, p = 0.046). The $\delta^{15}N_{bulk}$ values were relatively low ranging between 4‰ and 6‰ (Fig. 4d). During the Last Glacial Maximum, the $\delta^{15}N_{bulk}$ values were low, varying between 4.4‰ and 4.6‰, close to the typical mean range of dissolved nitrate in the ocean (Sigman et al., 1997). Subsequently, the $\delta^{15}N_{bulk}$ values increased from 16.7 ka BP (4.9‰), where we observed a decline in $[NO_3^-]_{BW}$ to 8.9 ka BP (5.6‰). The highest $\delta^{15}N_{bulk}$ values centered at ~14 ka BP (5.9‰). From 8.9 ka BP onwards, a long-term decrease in $\delta^{15}N_{bulk}$ (< 4.4‰) was observed until the Latest Holocene, consistent with higher $[NO_3^-]_{BW}$ levels during the Holocene (Fig. 4d). Despite higher $[NO_3^-]_{BW}$ levels, our reconstruction doesn't show any strong variations during the Holocene.

https://doi.org/10.5194/egusphere-2025-1182
Preprint. Discussion started: 25 March 2025

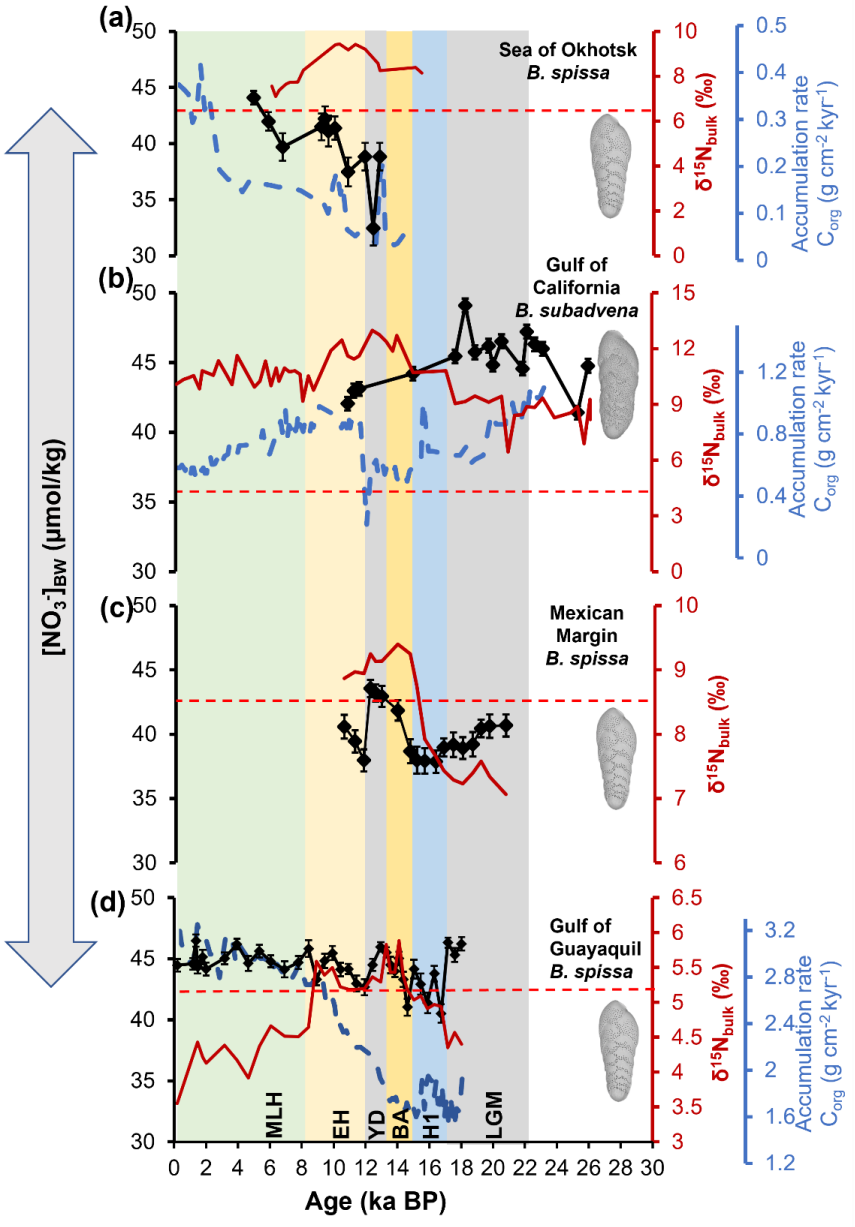

Figure 4. Quantitative $[NO_3^-]_{BW}$ reconstruction using the pore density of fossil specimens of *B. spissa*, *B. subadvena* from a) the Sea of Okhotsk (MD01-2415), b) the Gulf of California (DSDP-480), c) the Mexican Margin (MAZ-1E-04), and d) Gulf of Guayaquil (M77/2-59-01). The sedimentary nitrogen isotope ($\delta^{15}N_{bulk}$) records from the Sea of Okhotsk, and the Gulf of California are measured in this study, and the Gulf of Guayaquil is from Mollier-Vogel et al. (2019), and.

https://doi.org/10.5194/egusphere-2025-1182
Preprint. Discussion started: 25 March 2025

The $\delta^{15}N_{bulk}$ data for the Mexican Margin is from Alcorn et al. (2025). The error bars of $[NO_3^-]_{BW}$ represent 1 SEM including a complete error propagation (using equations 3 and 4). The accumulation rate of total organic carbon (Supplementary files) calculated from published literature (Bubenshchikova et al., 2015; Leclaire & Kerry, 1982; Mollier-Vogel et al., 2019) is shown in blue dashed lines for the Sea of Okhotsk, the Gulf of California and the Gulf of Guayaquil cores respectively. The red dashed lines indicate the modern nitrate concentration of each location. Time intervals Middle to Late Holocene (MLH), Early Holocene (EH), Younger Dryas (YD), Bølling-Allerød (BA), Heinrich Stadial 1 (H1), and Last Glacial Maximum (LGM) are shown in the figure.

3.5 Comparing the nitrate offset ($\Delta[NO_3^-]$) **between cores**. To quantify the change in $[NO_3^-]_{BW}$ between past and present conditions, we calculated the difference ($\Delta[NO_3^-]$ (µM)) between the modern $[NO_3^-]$ (Garcia et al., 2019) and the reconstructed past $[NO_3^-]_{BW}$ for each core. A $\Delta[NO_3^-]$ value close to 0 implies that there is no offset to the modern value. A positive (or negative) $\Delta[NO_3^-]$ implies higher (or lower) values than today. The Gulf of California had the highest $\Delta[NO_3^-]$ values relative to the other cores (see Fig. 5), and none of the values are close to the modern values. In general, the $\Delta[NO_3^-]$ values in the Gulf of California and mostly in the Gulf of Guayaquil were positive (Fig. 5) which indicated that bottom water NO_3^- concentrations in the past were higher than today in these regions. The Mexican Margin and the Sea of Okhotsk had negative $\Delta[NO_3^-]$, implying that NO_3^- concentrations in the past were lower than today (Fig. 5)

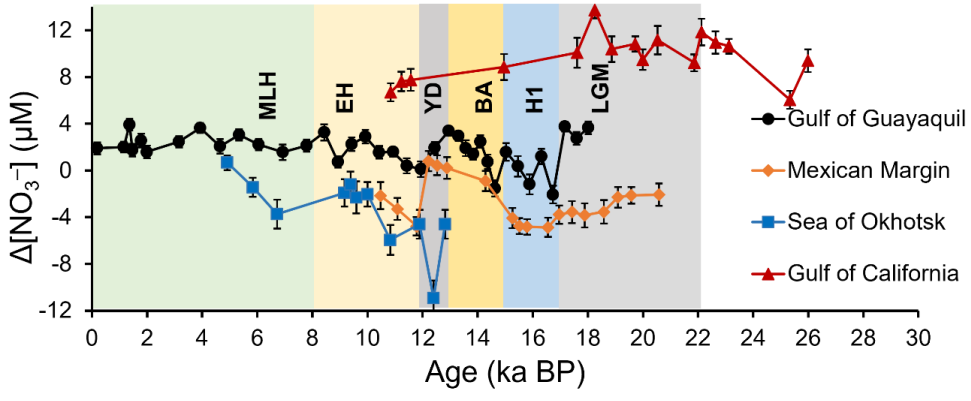

https://doi.org/10.5194/egusphere-2025-1182
Preprint. Discussion started: 25 March 2025

Figure 5. The nitrate offset ($\Delta[NO_3^-]$ (µM)) revealing changes of bottom water nitrate concentrations over the last 30 kyrs. The $[NO_3^-]_{BW}$ were calculated from the pore density of the benthic foraminifera *B. spissa* and *B. subadvena* from all studied cores compared to modern NO_3^- concentrations at each location. The modern nitrate (Table 1 and see fig. 4) at the different locations has been taken from the World Ocean Atlas, 2018 (Garcia et al., 2019). Error bars represent 1 SEM.

4. Discussion

Reconstruction of past $[NO_3^-]_{BW}$ in the ODZs is crucial for understanding the complex marine nitrogen cycle, and the processes/or factors involved in marine nutrient cycling. The comparison between past and modern NO_3^- will provide a foresight on the ecological and environmental impacts of climate change in these regions.

4.1 Sea of Okhotsk. Our data show that $[NO_3^-]_{BW}$ levels gradually increased through time and reached modern concentrations during the Middle-Holocene (Fig. 4a). Most of the nutrients in the northwestern Pacific including the Sea of Okhotsk are supplied by the upwelling of the North Pacific Deep Water (NPDW) (Gorbarenko et al., 2014). The weakened Kuroshio current (Ujiié and Ujiié, 1999) and increased sea ice extent (Ternois et al., 2001) weakened the upwelling of NPDW during the Last Glacial Maximum (LGM). Subsequent studies (Gray et al., 2020; Rae et al., 2020) have shown that the expansion of the North Pacific Gyre also resulted in less upwelling of NPDW during the LGM.

During the LGM, the subpolar North Pacific was better ventilated at intermediate depths (Keigwin, 1998) and export productivity was reduced (Ternois et al., 2001; Narita et al., 2002; Seki et al., 2004). This is consistent with a strengthened meridional overturning circulation, with enhanced formation of intermediate waters and advection of nutrient-depleted subtropical waters to high latitudes (Rae et al., 2020). Furthermore, the North Pacific subpolar gyre extended ~3° further south during the LGM (Gray et al., 2020), which shifted the westerly winds southward. This may have resulted in less upwelling of the NPDW during the LGM.

The prolonged ice cover with low biological productivity (Ternois et al., 2001; Narita et al., 2002; Seki et al., 2004; Rae et al., 2020) and well-oxygenated water masses (Keigwin, 1998) might have prevented the formation of an oxygen deficient zone (ODZ) in the Sea of Okhotsk

https://doi.org/10.5194/egusphere-2025-1182
Preprint. Discussion started: 25 March 2025

(Bubenshchikova et al., 2015). This is supported by the absence of *B. spissa*, which are adapted to living in dysoxic conditions, in our records during the LGM.

Deglacial low $[NO_3^-]_{BW}$ which correspond to higher $\delta^{15}N_{bulk}$ values (Fig. 4a) could be due to enhanced primary productivity. Increased nutrient supply from the Asian continental shelves and sea-ice retreat (Ternois et al., 2001) strengthened primary productivity. Indeed, the accumulation rate of total organic carbon was relatively higher during the Younger Dryas (Bubenshchikova et al., 2015) in our core (Fig. 4a). The increased oxygen demand and weakened ventilation of intermediate waters in the subarctic Pacific (Lembke-Jene et al., 2018) gradually intensified the ODZ. These poorly oxygenated conditions conceivably strengthened denitrification, resulting in low deglacial $[NO_3^-]_{BW}$ levels. However, during the Middle to Late Holocene (MLH) a reorganization in atmospheric circulation favored enhanced formation of oxygenated North Pacific Intermediate Water (NPIW) (Wang et al., 2020). Thus, mid-depth ventilation was closely associated with atmospheric circulation in the Holocene and a weakened ODZ (Ohkushi et al., 2013; Bubenshchikova et al., 2015; Wang et al., 2020). These rising oxygen concentrations probably reduced denitrification (low $\delta^{15}N_{bulk}$) in the Sea of Okhotsk, resulting in higher $[NO_3^-]_{BW}$ comparable to today's conditions (Fig. 4 & 5). The $\delta^{15}N_{bulk}$ values show a maximum from 13 ka to 10 ka BP, which indicates increased water-column denitrification during that time. Nevertheless, the $[NO_3^-]_{BW}$ increased during this time, which indicates a decoupling from denitrification in the oxygen minimum in the water column and the $[NO_3^-]_{BW}$. This could be related to the sea level rise during that time (Waelbroeck et al., 2008), which increased the vertical distance of the sediments (i.e., bottom water) at the sampling site from the center of denitrification.

4.2 Gulf of California. The Gulf of California ODZ is influenced by both intermediate and deep-water properties, similar to that of the open Pacific Ocean. Thus, the ODZ intensity in the Guaymas Basin is largely dependent on the oxygen content and ventilation of inflowing NPIW from the Sea of Okhotsk (Pride et al., 1999) and the demand for oxygen at depth. During the glacial period, the dissolved oxygen concentrations were higher due to better-ventilated NPIW at intermediate depths of the Northeast Pacific (Keigwin and Jones, 1990; Ganeshram et al., 1995; Keigwin 1998; Duplessy et al., 1988; Herguera et al., 2010; Cartapanis et al., 2011). Modeling studies show that the Laurentide and Cordilleran ice sheets increased in size (Benson et al., 2003), lowering the temperature of North America (Romanova et al., 2006) during the glacial period. The cold sinking air over the ice shee established a semi-permanent high-pressure cell (Kutzbach & Wright Jr, 1985;

https://doi.org/10.5194/egusphere-2025-1182
Preprint. Discussion started: 25 March 2025

Romanova et al., 2006) causing a substantially weaker North Pacific High (Ganeshram and Pedersen, 1998) or the southward displacement of the Inter Tropical Convergence Zone (Cheshire and Thurow, 2013). This resulted in a weak California Current along the coast and reduced upwelling-favorable winds (COHMAP et al., 1988; Cartapanis et al., 2011) along the North American coastline and reduced primary productivity (Ganeshram and Pedersen, 1998; Hendy et al., 2004; Cartapanis et al., 2011; Chang et al., 2015) within the ETNP and the Gulf of California during the glacial period. The nitrogen isotope ratios in the Guaymas Basin can be affected by subsurface denitrification in the Gulf and in the ETNP (Pride et al 1999). The increase in dissolved oxygen during the glacial period might have reduced water column denitrification (low $\delta^{15}N_{bulk}$) thereby increasing the $[NO_3^-]_{BW}$ (Fig. 4b).

Our study finds a declining trend in reconstructed $[NO_3^-]_{BW}$ during the Early Holocene, slowly approaching modern concentrations. This coincides with a maximum in $\delta^{15}N_{bulk}$ values, suggesting elevated denitrification. This agrees with previous studies in the ETNP (Kienast et al., 2002) and within the Gulf of California (Pride et al., 1999), which showed that high denitrification most likely was associated with warming temperatures that occurred during this period. Furthermore, the scarcity of benthic foraminifera after the Early Holocene in our study coincides with laminations of the sediment core (Keigwin & Jones, 1990) below 10.8 ka BP, where reconstructed $[NO_3^-]_{BW}$ begins to decrease. It is possible that redox conditions were too hostile for benthic foraminifers in the time periods when laminated sediments formed.

4.3 Mexican Margin. Our study finds a steep rise in $[NO_3^-]_{BW}$ between the Bølling-Allerød (BA) and the Younger Dryas (YD) (Fig. 4c). The transition period from the BA to the Holocene involved rapid oxygenation with increased oxygen levels at the onset of the YD (Jaccard & Galbraith, 2012; Ohkushi et al., 2013; Taylor et al., 2017). This has been linked to active ventilation by increased NPIW production at high latitudes in the North Pacific (Van Geen et al., 1996; Emmer and Thunell, 2000; Okazaki et al., 2010; Cartapanis et al., 2011; Chang et al., 2014). In addition, there was low primary productivity (Hendy et al., 2004; Pospelova et al., 2015), and a higher influx of freshwater (Broecker et al., 1985; Clark et al., 2002) during the YD. However, considering the deep location of the Mexican Margin core below the direct influence of intermediate water masses (Fig. 3), it is less likely to be reflected in the $[NO_3^-]_{BW}$. Bulk sediment $\delta^{15}N$ records in the ETNP (Ganeshram et al., 1995; Pride et al., 1999; Emmer and Thunell, 2000; S. S. Kienast et al., 2002; Hendy et al., 2004) found a decrease in $\delta^{15}N_{bulk}$ during the YD due to reduced denitrification. Furthermore, a

https://doi.org/10.5194/egusphere-2025-1182
Preprint. Discussion started: 25 March 2025

foraminifera-bound nitrogen isotope ($\delta^{15}N_{FB}$) study (Studer et al., 2021) in the eastern tropical Pacific also found a decrease in $\delta^{15}N_{FB}$ signatures during the Younger Dryas (Fig. 4c). In contrast to this, a bulk sediment $\delta^{15}N$ record of MAZ-1E-04 (Alcorn et al., 2025) depicts an increase in water column denitrification during the Younger Dryas. Thus, reduced denitrification may not be the dominant factor that led to the elevated $[NO_3^-]_{BW}$ during this time. Instead, the Mexican Margin may be more influenced by the NO_3^- variability from the Pacific Deep Water, PDW (see Fig. 3). Deep-sea reorganization and ventilation during the deglaciation may have influenced the $[NO_3^-]_{BW}$. At the onset of the deglaciation, deep Southern Ocean ventilation (reduced ^{14}C ventilation ages) and atmospheric carbon dioxide (CO_2) synchronously increased (Robinson et al., 2009; Burke and Robinson, 2012; Rae et al., 2018). This deglacial increase in ^{14}C ventilation in the Pacific Ocean suggests that most of the increase in atmospheric CO_2 is derived from old carbon in the Southern and Pacific Oceans (Rafter et al., 2022). The increase in reconstructed $[NO_3^-]_{BW}$ during the YD may thus reflect the release of sequestered nutrient- and carbon dioxide-rich waters during the deglaciation (Robinson et al., 2009; Rafter et al., 2022).

The relatively high $[NO_3^-]_{BW}$ during the glacial period (Fig. 4c), before its decline in Heinrich Stadial 1, is likely indicative of reduced water-column denitrification (Ganeshram et al., 1995; 2000) due to reduced productivity (Ganeshram et al., 1995; Ganeshram and Pedersen, 1998) and low organic matter flux through the oxygen minimum zone (Ganeshram et al., 2000). In the ETNP, including the Mexican Margin, coastal upwelling is driven by trade winds generated by subtropical high-pressure centers. These high-pressure centers largely result from differential heating of the land and the ocean. As a result of glacial cooling on land, these high-pressure systems and the associated trade winds that drive the upwelling have likely been weakened (Ganeshram and Pedersen, 1998).

4.4 Gulf of Guayaquil. The core M77/2-59-01 is in a region that is sensitive to changes in subsurface denitrification in the ETSP (Robinson et al., 2007, 2009; Dubois et al., 2011, 2014). The elevated reconstructed $[NO_3^-]_{BW}$ levels (Fig. 4d) during the glacial period suggest decreased water-column denitrification (Salvatteci et al., 2014; Erdem et al., 2020; Glock et al., 2022) and relatively low local productivity (Ganeshram et al., 2000; Robinson et al 2007; 2009; Martinez and Robinson et al., 2010; Salvatteci et al., 2016). Nutrient export to the deep Southern Ocean waters increased due to the sluggish Atlantic Meridional Overturning Circulation (Skinner et al., 2010), and increased atmospheric iron (Fe) deposition (Somes et al., 2017) during the glacial

https://doi.org/10.5194/egusphere-2025-1182
Preprint. Discussion started: 25 March 2025

period. This reduced the transport of preformed NO_3^- to the tropics via the Subantarctic Mode Water (SAMW), limiting productivity. In fact, the total organic carbon (Fig. 4d) depicts low productivity during this period. Furthermore, the colder sea surface temperature (SST) and the accelerated formation of SAMW and Antarctic Intermediate Water masses (Russell & Dickson, 2003; Galbraith et al., 2004) and the stronger high-latitude winds in the Southern Hemisphere (Karstensen and Quadfasel, 2002) increased the ventilation rate (Meissner et al., 2005; Jaccard and Galbraith, 2012; Muratli et al., 2010) during the glacial period. The resulting increased oxygen concentrations (Robinson et al., 2005; Robinson et al., 2007) decreased the volume of ODZs, and nitrogen loss processes (lower $\delta^{15}N_{bulk}$ values, Fig. 4d) during the glacial period. In addition, enhanced Fe deposition (Somes et al., 2017), and the glacial low sea level (Clark and Mix, 2002; Wallmann et al., 2016), may have influenced the nitrate inventory in the tropical and subtropical southern hemisphere.

A study by Glock et al. (2018) on core M77/2-52-2 from Peru applying the pore density of *B. spissa* also shows elevated $[NO_3^-]_{BW}$ during the Last Glacial Maximum, a similar decline in $[NO_3^-]_{BW}$ during the Heinrich Stadial 1 and thereafter a steady decrease in $[NO_3^-]_{BW}$ throughout the Holocene.

The deglacial decline in $[NO_3^-]_{BW}$, especially during Heinrich Stadial 1 in this study (Fig. 4d), indicates a gradual increase in surface productivity and bottom-water deoxygenation. High export production strengthened the expansion of the ETSP ODZ during the deglaciation as compared to LGM and MLH (Salvatteci et al., 2016; Glock et al., 2018; Mollier-Vogel et al., 2019). This is consistent with the denitrification signal in the Eastern Equatorial Pacific through westward advection from the Southeast Pacific margins (Martinez and Robinson, 2010).

The shift towards generally higher reconstructed $[NO_3^-]_{BW}$ from the Middle-Holocene, (Fig. 4d), implies a profound change in the climatic state of the Peruvian upwelling system and the associated ODZ during this time. From the deglaciation toward the Late Holocene, there was a general increase in productivity (Mollier-Vogel et al., 2019) as shown by organic carbon accumulation rates (Fig. 4d). This increase in organic matter input and/or preservation was likely related to an increase in upwelling-driven delivery of nutrients towards the surface. The gradual decrease in $\delta^{15}N_{bulk}$ values and higher $[NO_3^-]_{BW}$ was likely related to a relaxation in nutrient utilization with a nutrient supply exceeding the biological demand (Riechelson et al., 2024). Moreover, the core M77/2-59-01 was retrieved outside of the core ODZ and is under the strong influence of the oxygen

https://doi.org/10.5194/egusphere-2025-1182
Preprint. Discussion started: 25 March 2025

and nutrient-rich Equatorial Under Current subsurface waters (Salvatteci et al., 2019; Mollier-Vogel et al., 2019). These waters might have ventilated the Northern Peruvian margin and deepened the oxycline at this site during the Middle-Holocene. Furthermore, enhanced zonal SST (Koutavas et al., 2006) and a northward shift of the ITCZ strengthened the Pacific Walker and Hadley circulation during the Middle-Holocene across the tropical Pacific (Koutavas et al., 2006; Mollier-Vogel et al., 2013; Salvatteci et al., 2019). These enhanced atmospheric circulations brought oxygen-rich waters to intermediate depths off Peru via the equatorial subsurface countercurrents (Koutavas et al., 2006; Mollier-Vogel et al., 2013; Salvatteci et al., 2019). Hence, increased ventilation of subsurface water masses reduced the strength of nitrogen loss processes and nutrient uptake during the MLH.

4.5 Comparison of past and present [NO_3^-] at the studied locations. The [NO_3^-] during the present and past are compared to assess the resilience of our chosen study locations towards environmental and ecological impacts of climate change. The generally positive $\Delta[NO_3^-]$ that we found (Fig. 5) in the Gulf of California (Guaymas Basin) and the Gulf of Guayaquil indicate that today the [NO_3^-] is lower than in the past. This suggests that today the nitrogen loss processes at these two core sites are stronger, most likely related to ocean warming and a decline in oxygen concentration of bottom waters. The Gulf of California core is within the heart of the oxygen-deficient zone, and thus changes in ODZ oxygenation or denitrification will be more evident in this core than in any other core studied. Under nitrogen limitation, negative feedbacks (e.g., anammox) result in a decline in productivity (Naafs et al., 2019; Wallmann et al., 2022), which will stabilize the oxygen concentration. In the case of the Gulf of California, sediments are enriched in reactive iron (Fe) (Scholz et al., 2019). The decreasing NO_3^- concentrations in the bottom water reduce the flux of NO_3^- into the surface sediment. This leads to the release of sedimentary Fe, which enhances nitrogen fixation in the Guaymas Basin (Scholz et al., 2019). Thus, increased denitrification might not act as negative feedback in the Gulf of California because it might be countered by increased nitrogen fixation (White et al., 2013).

In the case of the Gulf of Guayaquil, whether today's elevated denitrification could enhance N_2 fixation also depends on the availability of Fe (Pennington et al., 2006). The primary productivity of the Peruvian ODZ is Fe limited due to the reduction of particular Fe oxides in shelf and slope sediments (Scholz et al., 2014). Modeling studies show that primary productivity will be amplified in the Peruvian ODZ due to the release of Fe from shelf and slope sediments (Wallmann et al.,

https://doi.org/10.5194/egusphere-2025-1182
Preprint. Discussion started: 25 March 2025

2022). This may induce deoxygenation and drive the expansion and intensification of Peruvian ODZ resulting in a positive feedback loop, like in the Gulf of California. This situation is indicated by lower $[NO_3^-]$ today compared to the past ~20,000 years (Fig. 5).

The negative nitrate $\Delta[NO_3^-]$ in the Sea of Okhotsk and the Mexican Margin (Fig. 5) indicates that modern $[NO_3^-]$ levels are higher than in the reconstructed past. This suggests that modern nitrogen loss is decreased at these two core sites compared to the last deglaciation. The higher modern $[NO_3^-]$ in the Sea of Okhotsk is likely associated with less primary productivity and more oxygen in the water column similar to the situation established in the MLH. The higher modern $[NO_3^-]_{BW}$ in the case of the Mexican Margin could be associated with sea level rise. The ODZ in the Mexican Continental Margin might have shifted to shallower depths today with less/or no benthic denitrification in intermediate water depths at the core site, resulting in high $[NO_3^-]_{BW}$ levels. During the glacial period, continental shelves were exposed due to sea-level lowstands (Clark and Mix, 2002; Kuhlmann et al., 2004; Wallmann et al., 2016), the main areas of primary productivity may have migrated offshore from the shallow shelf towards the continental slope relative to their Holocene positions. A similar situation occurred at the Benguela upwelling system during the LGM: TOC accumulation at the continental slope increased during the LGM in response to the seaward shift of centers of enhanced productivity (Mollenhauer et al., 2002). This offshore shift of the productivity centers and the most likely reduced remineralization rates, due to lower temperatures, indicate that the center of the ODZ at the Mexican Margin before sea level rise was possibly deeper than today. However, with the deglacial eustatic sea-level rise, the ODZ may have shifted to shallower depths. This shifted the main zone of denitrification further away from the seafloor, resulting in the increased modern $[NO_3^-]_{BW}$ in comparison to the LGM (Fig. 5).

5. Conclusion. The quantitative reconstruction of $[NO_3^-]_{BW}$ using the pore density of denitrifying benthic foraminifera over the last deglaciation at the four studied ODZs provides a comprehensive understanding of the past $[NO_3^-]$. Ocean deoxygenation and warming alter nutrient cycling and the functioning of marine ecosystems and food webs. Combining the relatively new pore density proxy of denitrifying foraminifera with $\delta^{15}N_{bulk}$ has the potential to further resolve the processes in the marine nitrogen cycle in oxygen deficient zones. The Gulf of Guayaquil and Gulf of California data shows elevated $[NO_3^-]_{BW}$ during the glacial period compared to deglacial and modern conditions. Considering the well-ventilated intermediate water masses in the Sea of

https://doi.org/10.5194/egusphere-2025-1182
Preprint. Discussion started: 25 March 2025

Okhotsk, the Sea of Okhotsk may have also elevated $[NO_3^-]_{BW}$ in the glacial period. For the Mexican Margin core, $[NO_3^-]_{BW}$ was particularly strong during the Younger Dryas. The reconstructed $[NO_3^-]_{BW}$ from the Sea of Okhotsk, the Gulf of California, and the Gulf of Guayaquil are influenced by the formation of the North Pacific Intermediate Water. However, the $[NO_3^-]_{BW}$ in the deeper site, the Mexican Margin is likely influenced by the NO_3^- variability in Pacific Deep Water. The modern Gulf of Guayaquil and the Gulf of California have low $[NO_3^-]$ associated with increased denitrification and a strengthening ODZ. In contrast, higher modern $[NO_3^-]$ was observed in the Sea of Okhotsk and the Mexican Margin, suggesting that these two study areas have higher oxygen.

Code and Data availability

All data generated or analyzed during this study are included in the tables of this published article (and its Supplementary information files).

Author contributions

A.G.M wrote the core manuscript, did the sample preparation, electron microscopy, image and statistical analyses of all the fossil foraminifera. N.G. planned the study design and sampling strategy. G.S. hosted the research group, and provided access to SEM, and lab facilities at the University of Hamburg. D.N. provided sampling material for cores MD01-2415 and M77/2-59-01. C.D. provided sampling material for core MAZ-1E-04. N.L., R.S., and A.B. facilitated the measurement of nitrogen isotopes in the sediment samples of core MD01-2415 and DSDP-480. R.A. contributed to the age model development of core MAZ-1E-04, and H.F helped in the image processing of core DSDP-480. All authors contributed to the discussion and preparation of the manuscript.

Competing interests

The authors declare no competing interests.

Acknowledgements

We are grateful to the micropaleontology group at the University of Hamburg, Germany. We thank Alfredo Martinez-Garcia, Max Planck Institute for Chemistry, Mainz, Germany for the support with the measurement of nitrogen isotopes in the sediment samples. We acknowledge the help of

https://doi.org/10.5194/egusphere-2025-1182
Preprint. Discussion started: 25 March 2025

Jutta Richarz, Kaya Oda for lab support, PhD student Sven Brömme (Max Planck Institute for Chemistry, Mainz) and student assistant Hannah Krüger. We thank Yvon Balut, Agnes Baltzer, and the Shipboard Scientific Party of RV Marion Dufresne cruise WEPAMA 2001 for their kind support. We thank IODP for providing the sample for core DSDP-480. The study is a contribution to the Center for Earth System Research and Sustainability (CEN) of University of Hamburg.

Financial support

Funding was provided by the Deutsche Forschungsgemeinschaft (DFG) through both N.G.'s Heisenberg grant GL 999/3-1 and grant GL 999/4-1. Funding for the core MD01-2415 recovery was provided by the German Science Foundation (DFG) within project Ti240/11-1. The recovery of core M77-59 recovery was a contribution of the German Science Foundation (DFG) Collaborative Research Project "Climate–Biogeochemistry interactions in the Tropical Ocean" (SFB 754).

References

1. Alcorn, R. C., Ontiveros-Cuadras, J. F., Menon, A. G., Glock, N., Tappa, E. J., Burke, J., ... & Davis, C. V. Nonlinear Expansion of the Eastern Tropical North Pacific Oxygen Minimum Zone During the Last Deglaciation. *Authorea Preprints* (2025).
2. Altabet, M. A., Pilskaln, C., Thunell, R., Pride, C., Sigman, D., Chavez, F., & Francois, R. The nitrogen isotope biogeochemistry of sinking particles from the margin of the Eastern North Pacific. Deep Sea Research Part I: Oceanographic Research Papers, 46(4), 655-679 (1999).
3. Altabet, M. A., & Francois, R. Sedimentary nitrogen isotopic ratio as a recorder for surface ocean nitrate utilization. Global biogeochemical cycles, 8(1), 103-116 (1994).
4. Auderset, A., Moretti, S., Taphorn, B., Ebner, P. R., Kast, E., Wang, X. T., ... & Martínez-García, A. Enhanced Ocean oxygenation during Cenozoic warm periods. Nature, 609(7925), 77-82 (2022).
5. Benson, L., Lund, S., Negrini, R., Linsley, B., & Zic, M. Response of north American Great basin lakes to Dansgaard–Oeschger oscillations. Quaternary Science Reviews, 22(21-22), 2239-2251 (2003).
6. Bernhard, J. M., Edgcomb, V. P., Casciotti, K. L., McIlvin, M. R., & Beaudoin, D. J.. Denitrification likely catalyzed by endobionts in an allogromiid foraminifer. The ISME journal, 6(5), 951-960 (2012a).
7. Bernhard, J. et al. Potential importance of physiologically diverse benthic foraminifera in sedimentary nitrate storage and respiration. J. Geophys. Res. 117 (2012b).
8. Bohlen, L., Dale, A. W., & Wallmann, K.. Simple transfer functions for calculating benthic fixed nitrogen losses and C: N: P regeneration ratios in global biogeochemical models. *Global biogeochemical cycles*, *26*(3) (2012)

https://doi.org/10.5194/egusphere-2025-1182
Preprint. Discussion started: 25 March 2025

9. Broecker, W. S., Peteet, D. M., & Rind, D. Does the ocean–atmosphere system have more than one stable mode of operation? Nature, 315(6014), 21-26 (1985).
10. Bubenshchikova, N., Nürnberg, D., & Tiedemann, R. Variations of Okhotsk Sea oxygen minimum zone: Comparison of foraminiferal and sedimentological records for latest MIS 12–11c and latest MIS 2–1. Marine Micropaleontology, 121, 52-69 (2015).
11. Burke, A., & Robinson, L. F. The Southern Ocean's role in carbon exchange during the last deglaciation. science, 335(6068), 557-561 (2012).
12. Butzin, M., Heaton, T. J., Köhler, P., & Lohmann, G. A short note on marine reservoir age simulations used in IntCal20. Radiocarbon, 62(4), 865-871 (2020).
13. Cartapanis, O., Tachikawa, K., & Bard, E. Northeastern Pacific oxygen minimum zone variability over the past 70 kyr: Impact of biological production and oceanic ventilation. Paleoceanography, 26(4) (2011).
14. Casciotti, K. L. Nitrite isotopes as tracers of marine N cycle processes. Philos. Trans. R. Soc. A 374:20150295 (2016).
15. Chang, A. S., Pedersen, T. F., & Hendy, I. L. Effects of productivity, glaciation, and ventilation on late Quaternary sedimentary redox and trace element accumulation on the Vancouver Island margin, western Canada. Paleoceanography, 29(7), 730–746 (2014).
16. Chang, A. S., Pichevin, L., Pedersen, T. F., Gray, V., & Ganeshram, R. New insights into productivity and redox-controlled trace element (Ag, Cd, Re, and Mo) accumulation in a 55 kyr long sediment record from Guaymas Basin, Gulf of California. Paleoceanography, 30(2), 77-94 (2015).
17. Cheshire, H., & Thurow, J. High-resolution migration history of the Subtropical High/Trade Wind system of the northeastern Pacific during the last~ 55 years: Implications for glacial atmospheric reorganization. Paleoceanography, 28(2), 319-333 (2013).
18. Clark, P. U., & Mix, A. C. Ice sheets and sea level of the Last Glacial Maximum. Quaternary Science Reviews, 21(1-3), 1-7 (2002).
19. Clark, P., Pisias, N., Stocker, T. et al. The role of the thermohaline circulation in abrupt climate change. Nature 415, 863–869 (2002).
20. Codispoti, L. A. et al. The oceanic fixed nitrogen and nitrous oxide budgets: Moving targets as we enter the anthropocene? Sci. Mar. 65, 85–105 (2001).
21. Cohmap Members. Climatic changes of the last 18,000 years: observations and model simulations. Science, 241(4869), 1043-1052 (1988).
22. Curray, Joseph R; Moore, David G; Kelts, Kerry; Einsele, Gerhard (1982): Compilation of detailed examination of Mn deposits from the North tip of the Baja peninsula prior to DSDP Leg 64 [dataset]. PANGAEA, https://doi.org/10.1594/PANGAEA.874590, Supplement to: Curray, JR et al. (1982): Tectonics and Geological History of the Passive Continental Margin at the Tip of Baja California. In: Curray, J.R.; Moore, D.G.; et al., Initial Reports of the Deep Sea Drilling Project, U.S. Government Printing Office, LXIV, 1089-1136, https://doi.org/10.2973/dsdp.proc.64.150.1982
23. Dale, A. W., Sommer, S., Lomnitz, U., Bourbonnais, A. & Wallmann, K. Biological nitrate transport in sediments on the Peruvian margin mitigates benthic sulfide emissions and drives pelagic N loss during stagnation events. Deep Res. I Oceanogr. Res. Pap. 112, 123–136 (2016).
24. Deutsch, C., Sigman, D.M., Thunell, R. C.,Meckler, A. N., and Haug, G. H. Isotopic constraints on glacial/interglacial changes in the oceanic nitrogen budget. Global Biogeochem. Cycles 18, GB4012 (2004).

https://doi.org/10.5194/egusphere-2025-1182
Preprint. Discussion started: 25 March 2025

25. Devol, A. H., Uhlenhopp, A. G., Naqvi, S. W. A., Brandes, J. A., Jayakumar, D. A., Naik, H., ... & Yoshinari, T. Denitrification rates and excess nitrogen gas concentrations in the Arabian Sea oxygen deficient zone. Deep Sea Research Part I: Oceanographic Research Papers, 53(9), 1533-1547 (2006).
26. Dubois, N., Kienast, M., Kienast, S., Normandeau, C., Calvert, S. E., Herbert, T. D., & Mix, A. Millennial-scale variations in hydrography and biogeochemistry in the Eastern Equatorial Pacific over the last 100 kyr. Quaternary Science Reviews, 30(1–2), 210–223 (2011).
27. Dubois, N., Kienast, M., Kienast, S. S., & Timmermann, A. Millennial-scale Atlantic/East Pacific Sea surface temperature linkages during the last 100,000 years. Earth and Planetary Science Letters, 396, 134–142 (2014).
28. Duplessy, J. C., Shackleton, N. J., Fairbanks, R. G., Labeyrie, L., Oppo, D., & Kallel, N. Deepwater source variations during the last climatic cycle and their impact on the global deepwater circulation. Paleoceanography, 3(3), 343-360 (1988).
29. Emmer, E., & Thunell, R. C. Nitrogen isotope variations in Santa Barbara Basin sediments: Implications for denitrification in the eastern tropical North Pacific during the last 50,000 years. Paleoceanography, 15(4), 377-387 (2000).
30. Erdem, Z., Schönfeld, J., Rathburn, A. E., Pérez, M. E., Cardich, J., & Glock, N. Bottom-water deoxygenation at the Peruvian margin during the last deglaciation recorded by benthic foraminifera. Biogeosciences, 17(12), 3165-3182 (2020).
31. Eugster, O., Gruber, N., Deutsch, C., Jaccard, S. L., and Payne, M. R. The dynamics of the marine nitrogen cycle across the last deglaciation. Paleoceanography 28, 116–129 (2013).
32. Evans, N., Tichota, J., Ruef, W., Moffett, J., & Devol, A. Rapid Expansion of Fixed Nitrogen Deficit in the Eastern Pacific Ocean Revealed by 50-Year Time Series. Global Biogeochemical Cycles, 37(10), e2022GB007575 (2023).
33. Fontanier, C. et al. Living (stained) deep-sea foraminifera off hachinohe (NE Japan, western Pacific): Environmental interplay in oxygen-depleted ecosystems. J. Foraminifer. Res. 44, 281–299 (2014).
34. Frölicher, T. L., Aschwanden, M. T., Gruber, N., Jaccard, S. L., Dunne, J. P., & Paynter, D. Contrasting upper and deep ocean oxygen response to protracted global warming. Global biogeochemical cycles, 34(8), e2020GB006601 (2020).
35. Fu, W., Primeau, F., Keith Moore, J., Lindsay, K., & Randerson, J. T. Reversal of increasing tropical ocean hypoxia trends with sustained climate warming. Global Biogeochemical Cycles, 32(4), 551-564 (2018).
36. Galbraith, E. D., Kienast, M., Pedersen, T. F., & Calvert, S. E. Glacial-interglacial modulation of the marine nitrogen cycle by high-latitude O2 supply to the global thermocline. Paleoceanography, 19(4) (2004).
37. Ganeshram, R. S., & Pedersen, T. F. Glacial-interglacial variability in upwelling and bioproductivity off NW Mexico: Implications for quaternary paleoclimate. Paleoceanography, 13(6), 634-645 (1998).
38. Ganeshram, R. S., Pedersen, T. F., Calvert, S. E., & Murray, J. W. Large changes in oceanic nutrient inventories from glacial to interglacial periods. Nature, 376(6543), 755-758 (1995).
39. Ganeshram, R. S., Pedersen, T. F., Calvert, S. E., McNeill, G. W., & Fontugne, M. R. Glacial-interglacial variability in denitrification in the world's oceans: Causes and consequences. Paleoceanography, 15(4), 361-376 (2000).

https://doi.org/10.5194/egusphere-2025-1182
Preprint. Discussion started: 25 March 2025

40. Ganeshram, R. S., Pedersen, T. F., Calvert, S., & François, R. Reduced nitrogen fixation in the glacial ocean inferred from changes in marine nitrogen and phosphorus inventories. Nature, 415(6868), 156-159 (2002).
41. Garcia H.E., Boyer, T. P., Baranova, O. K., Locarnini, R.A., Mishonov, A.V., Grodsky, A., Paver, C.R., Weathers, K.W., Smolyar, I.V., Reagan, J.R., Seidov, M.M., Zweng, D., World Ocean Atlas 2018: Product documentation. A. Mishonov, Technical Editor (2019).
42. Glock, N. et al. Coupling of oceanic carbon and nitrogen facilitates spatially resolved quantitative reconstruction of nitrate inventories. Nat. Commun. 9, 1217 (2018).
43. Glock, N. et al. Environmental influences on the pore density of *Bolivina spissa* (Cushman). J. Foraminifer. Res. 41, 22–32 (2011).
44. Glock, N. et al. Metabolic preference of nitrate over oxygen as an electron acceptor in foraminifera from the Peruvian oxygen minimum zone. Proc. Natl. Acad. Sci. U. S. A. 116, 2860–2865 (2019).
45. Glock, N. et al. The role of benthic foraminifera in the benthic nitrogen cycle of the Peruvian oxygen minimum zone. Biogeosciences 10, 4767–4783 (2013).
46. Glock, N., Erdem, Z., & Schönfeld, J. The Peruvian oxygen minimum zone was similar in extent but weaker during the Last Glacial Maximum than Late Holocene. Communications Earth & Environment, 3(1), 307 (2022).
47. Goodfriend, G. A., & Flessa, K. W. Radiocarbon reservoir ages in the Gulf of California: roles of upwelling and flow from the Colorado River. Radiocarbon, 39(2), 139-148 (1997).
48. Goldstein, S. T. Foraminifera: A biological overview. Mod. Foraminifera 37–55 doi:10.1007/0-306-48104-9_3 (1999).
49. Gomaa, F., Utter, D. R., Powers, C., Beaudoin, D. J., Edgcomb, V. P., Filipsson, H. L., ... & Bernhard, J. M. Multiple integrated metabolic strategies allow foraminiferan protists to thrive in anoxic marine sediments. Science Advances, 7(22), eabf1586 (2021).
50. Gorbarenko, S. A., Artemova, A. V., Goldberg, E. L., & Vasilenko, Y. P. The response of the Okhotsk Sea environment to the orbital-millennium global climate changes during the Last Glacial Maximum, deglaciation and Holocene. Global and Planetary Change, 116, 76-90 (2014).
51. Govindankutty Menon, A., Davis, C.V., Nürnberg, D. et al. A deep-learning automated image recognition method for measuring pore patterns in closely related bolivinids and calibration for quantitative nitrate paleo-reconstructions. Sci Rep 13, 19628 (2023).
52. Gray, W. R., Wills, R. C., Rae, J. W., Burke, A., Ivanovic, R. F., Roberts, W. H., ... & Valdes, P. J. Wind-driven evolution of the North Pacific subpolar gyre over the last deglaciation. Geophysical Research Letters, 47(6), e2019GL086328 (2020).
53. Gruber, N. & Galloway, J. N. An earth-system perspective of the global nitrogen cycle. Nature 451, 293–296 (2008).
54. Gruber, N. The marine nitrogen cycle: overview and challenges. Nitrogen in the marine environment, 2, 1-50 (2008).
55. Haslett J, Parnell AC. "A simple monotone process with application to radiocarbon-dated depth chronologies." Journal of the Royal Statistical Society: Series C (Applied Statistics), 57(4), 399–418 (2008).
56. Heaton, T. J., Köhler, P., Butzin, M., Bard, E., Reimer, R. W., Austin, W. E., ... & Skinner, L. C. Marine20—the marine radiocarbon age calibration curve (0–55,000 cal BP). Radiocarbon, 62(4), 779-820 (2020).

https://doi.org/10.5194/egusphere-2025-1182
Preprint. Discussion started: 25 March 2025

57. Hendy, I. L., Pedersen, T. F., Kennett, J. P., & Tada, R. Intermittent existence of a southern Californian upwelling cell during submillennial climate change of the last 60 kyr. Paleoceanography, 19(3) (2004).
58. Herguera, J. C., Herbert, T., Kashgarian, M., & Charles, C. Intermediate and deep-water mass distribution in the Pacific during the Last Glacial Maximum inferred from oxygen and carbon stable isotopes. Quaternary Science Reviews, 29(9-10), 1228-1245 (2010).
59. Hess, A. V., Auderset, A., Rosenthal, Y., Miller, K. G., Zhou, X., Sigman, D. M., & Martínez-García, A. A well-oxygenated eastern tropical Pacific during the warm Miocene. Nature, 619(7970), 521-525 (2023).
60. Holbourn, A., Kiefer, T., Pflaumann, U., & Rothe, S. WEPAMA Cruise MD 122/IMAGES VII, Rapp. Campagnes Mer OCE/2002/01, Inst. Polaire Fr. Paul Emile Victor (IPEV), Plouzane, France (2002).
61. Jaccard, S., Galbraith, E. Large climate-driven changes of oceanic oxygen concentrations during the last deglaciation. Nature Geosci 5, 151–156 (2012).
62. Kamp, A., Høgslund, S., Risgaard-Petersen, N., & Stief, P.. Nitrate storage and dissimilatory nitrate reduction by eukaryotic microbes. Frontiers in microbiology, 6, 1492 (2015).
63. Karstensen, J., & Quadfasel, D. Formation of Southern Hemisphere thermocline waters: Water mass conversion and subduction. Journal of Physical Oceanography, 32(11), 3020-3038 (2002).
64. Keeling, R. F., Kortzinger, A. & Gruber, N. Ocean deoxygenation in a warming world. Ann. Rev.Mar. Sci. 2, 199–229 (2010).
65. Keigwin, L. D. Glacial-age hydrography of the far northwest Pacific Ocean. Paleoceanography, 13(4), 323-339 (1998).
66. Keigwin, L. D., & Jones, G. A. Deglacial climatic oscillations in the Gulf of California. Paleoceanography, 5(6), 1009-1023 (1990).
67. Kienast, S. S., Calvert, S. E., & Pedersen, T. F. Nitrogen isotope and productivity variations along the northeast Pacific margin over the last 120 kyr: Surface and subsurface paleoceanography. Paleoceanography, 17(4), 7-1 (2002).
68. Kienast, M., Higginson, M. J., Mollenhauer, G., Eglinton, T. I., Chen, M. T., & Calvert, S. E.. On the sedimentological origin of down-core variations of bulk sedimentary nitrogen isotope ratios. Paleoceanography, 20(2) (2005).
69. Koutavas, A., Demenocal, P. B., Olive, G. C., & Lynch-Stieglitz, J. Mid-Holocene El Niño–Southern Oscillation (ENSO) attenuation revealed by individual foraminifera in eastern tropical Pacific sediments. Geology, 34(12), 993-996 (2006).
70. Kuhlmann, H., Freudenthal, T., Helmke, P., & Meggers, H.. Reconstruction of paleoceanography off NW Africa during the last 40,000 years: influence of local and regional factors on sediment accumulation. *Marine Geology*, *207*(1-4), 209-224 (2004).
71. Kutzbach, J. E., & Wright Jr, H. E. Simulation of the climate of 18,000 years BP: Results for the North American/North Atlantic/European sector and comparison with the geologic record of North America. Quaternary Science Reviews, 4(3), 147-187 (1985).
72. Kuzmin, Y. V., Burr, G. S., Gorbunov, S. V., Rakov, V. A., & Razjigaeva, N. G. A tale of two seas: reservoir age correction values (R, ΔR) for the Sakhalin Island (Sea of Japan and Okhotsk Sea). Nuclear Instruments and Methods in Physics Research Section B: Beam Interactions with Materials and Atoms, 259(1), 460-462 (2007).
73. Lam, P. & Kuypers, M. M. M. Microbial nitrogen cycling processes in oxygen minimum zones. Ann. Rev. Mar. Sci. 3, 317–345 (2011).

https://doi.org/10.5194/egusphere-2025-1182
Preprint. Discussion started: 25 March 2025

903 74. Leclaire, J., & Kerry, K. Calcium carbonate and organic carbon stratigraphy of late Quaternary
904 laminated and homogeneous diatom oozes from the Guaymas Slope, HPC Site 480, Gulf of
905 California (1982).
906 75. Lembke-Jene, L., Tiedemann, R., Nürnberg, D., Gong, X., & Lohmann, G. Rapid shift and
907 millennial-scale variations in Holocene North Pacific Intermediate Water ventilation.
908 Proceedings of the National Academy of Sciences, 115(21), 5365-5370 (2018).
909 76. Levin LA.. Oxygen minimum zone benthos: Adaptation and community response to hypoxia.
910 In Oceanography and Marine Biology, vol. 41, pp. 1–45 (2003).
911 77. Levin, L. A. Manifestation, drivers, and emergence of open ocean deoxygenation. Annual
912 review of marine science, 10(1), 229-260 (2018).
913 78. Li, N., Somes, C. J., Landolfi, A., Chien, C. T., Pahlow, M., & Oschlies, A. Global impact of
914 benthic denitrification on marine N2 fixation and primary production simulated by a variable-
915 stoichiometry Earth system model. EGUsphere, 2024, 1-30 (2024).
916 79. Liu, K. K., & Kaplan, I. R. The eastern tropical Pacific as a source of 15N-enriched nitrate in
917 seawater off southern California. Limnology and Oceanography, 34(5), 820-830 (1989).
918 80. Lourey, M. J., Trull, T. W., & Sigman, D. M. Sensitivity of δ15N of nitrate, surface
919 suspended and deep sinking particulate nitrogen to seasonal nitrate depletion in the Southern
920 Ocean. Global Biogeochemical Cycles, 17(3) (2003).
921 81. Martinez, P., & Robinson, R. S. Increase in water column denitrification during the last
922 deglaciation: the influence of oxygen demand in the eastern equatorial Pacific. Biogeosciences,
923 7(1), 1-9 (2010).
924 82. Meckler, A. N., Ren, H., Sigman, D. M., Gruber, N., Plessen, B., Schubert, C. J., & Haug, G.
925 H.. Deglacial nitrogen isotope changes in the Gulf of Mexico: Evidence from bulk sedimentary
926 and foraminifera-bound nitrogen in Orca Basin sediments. Paleoceanography, 26(4) (2011).
927 83. Meissner, K. J., Galbraith, E. D., & Völker, C. Denitrification under glacial and interglacial
928 conditions: A physical approach. Paleoceanography, 20(3) (2005).
929 84. Mollenhauer, G., Schneider, R. R., Müller, P. J., Spieß, V., & Wefer, G. Glacial/interglacial
930 variablity in the Benguela upwelling system: Spatial distribution and budgets of organic carbon
931 accumulation. Global Biogeochemical Cycles, 16(4), 81-1 (2002).
932 85. Mollier-Vogel, E. et al. Mid-holocene deepening of the Southeast Pacific oxycline. Glob.
933 Planet. Change 172, 365–373 (2019).
934 86. Mollier-Vogel, E., Leduc, G., Böschen, T., Martinez, P., & Schneider, R. R.. Rainfall response
935 to orbital and millennial forcing in northern Peru over the last 18 ka. Quaternary Science
936 Reviews, 76, 29-38 (2013).
937 87. Montoya, J. P., Horrigan, S. G., & McCarthy, J. J. Natural abundance of ^{15}N in particulate
938 nitrogen and zooplankton in the Chesapeake Bay. Marine Ecology Progress Series, 35-61
939 (1990).
940 88. Moore, C.M., Mills, M.M., Arrigo, K. R., Berman-Frank, I., Bopp, L., Boyd, P.W., et al.
941 Processes and patterns of oceanic nutrient limitation. Nat. Geosci.6, 701–710 (2013).
942 89. Moretti, S., Auderset, A., Deutsch, C., Schmitz, R., Gerber, L., Thomas, E., ... & Martínez-
943 García, A. Oxygen rise in the tropical upper ocean during the Paleocene-Eocene Thermal
944 Maximum. Science, 383(6684), 727-731 (2024).
945 90. Muratli, J. M., Chase, Z., Mix, A. C., & McManus, J. Increased glacial-age ventilation of the
946 Chilean margin by Antarctic Intermediate Water. Nature Geoscience, 3(1), 23-26 (2010).
947 91. Naafs, B. D. A., Monteiro, F. M., Pearson, A., Higgins, M. B., Pancost, R. D., & Ridgwell,
948 A. Fundamentally different global marine nitrogen cycling in response to severe ocean

https://doi.org/10.5194/egusphere-2025-1182
Preprint. Discussion started: 25 March 2025

deoxygenation. Proceedings of the National Academy of Sciences, 116(50), 24979-24984 (2019).
92. Narita, H., Sato, M., Tsunogai, S., Murayama, M., Ikehara, M., Nakatsuka, T., ... & Ujiié, Y. Biogenic opal indicating less productive northwestern North Pacific during the glacial ages. Geophysical Research Letters, 29(15), 22-1 (2002).
93. Nürnberg, D. & Tiedemann, R. Environmental change in the Sea of Okhotsk during the last 1.1 million years. Paleoceanography 19, 1–23 (2004).
94. Nürnberg, D. et al. Sea surface and subsurface circulation dynamics off equatorial Peru during the last ~17 kyr. Paleoceanography 30 (7), 984–999 (2015).
95. Ohkushi, K., Kennett, J. P., Zeleski, C. M., Moffitt, S. E., Hill, T. M., Robert, C., ... & Behl, R. J. Quantified intermediate water oxygenation history of the NE Pacific: A new benthic foraminiferal record from Santa Barbara basin. Paleoceanography, 28(3), 453-467 (2013).
96. Okazaki, Y., Timmermann, A., Menviel, L., Harada, N., Abe-Ouchi, A., Chikamoto, M. O., ... & Asahi, H. Deepwater formation in the North Pacific during the last glacial termination. Science, 329(5988), 200-204 (2010).
97. Orsi, W.D., Morard, R., Vuillemin, A. et al. Anaerobic metabolism of Foraminifera thriving below the seafloor. ISME J 14, 2580–2594 (2020).
98. Oschlies, A. A committed fourfold increase in ocean oxygen loss. Nat Commun 12, 2307 (2021).
99. Pennington, J. T., Mahoney, K. L., Kuwahara, V. S., Kolber, D. D., Calienes, R., & Chavez, F. P. Primary production in the eastern tropical Pacific: A review. *Progress in oceanography*, *69*(2-4), 285-317 (2006).
100. Piña-Ochoa, E. et al. Widespread occurrence of nitrate storage and denitrification among Foraminifera and Gromiida. Proc. Natl. Acad. Sci. U.S.A. 107, 1148–1153 (2010a).
101. Piña-Ochoa, E., Koho, K. A., Geslin, E. & Risgaard-Petersen, N. Survival and life strategy of the foraminiferan Globobulimina turgida through nitrate storage and denitrification. Mar. Ecol. Prog. Ser. 417, 39–49 (2010b).
102. Pospelova, V., Price, A. M., & Pedersen, T. F. Palynological evidence for late Quaternary climate and marine primary productivity changes along the California margin. Paleoceanography, 30(7), 877-894 (2015).
103. Pride, C. J. An evaluation and application of paleoceanographic proxies in the Gulf of California. University of South Carolina (1997).
104. Pride, C., Thunell, R., Sigman, D., Keigwin, L., Altabet, M., & Tappa, E. Nitrogen isotopic variations in the Gulf of California since the last deglaciation: Response to global climate change. Paleoceanography, 14(3), 397-409 (1999).
105. Rae, J. W., Gray, W. R., Wills, R. C. J., Eisenman, I., Fitzhugh, B., Fotheringham, M., ... & Burke, A. Overturning circulation, nutrient limitation, and warming in the Glacial North Pacific. Science advances, 6(50), eabd1654 (2020).
106. Rae, J.W.B., Burke, A., Robinson, L.F. et al. CO2 storage and release in the deep Southern Ocean on millennial to centennial timescales. Nature 562, 569–573 (2018).
107. Rafter, P. A., Gray, W. R., Hines, S. K., Burke, A., Costa, K. M., Gottschalk, J., ... & DeVries, T. Global reorganization of deep-sea circulation and carbon storage after the last ice age. Science Advances, 8(46), eabq5434 (2022).
108. Ren, H., Sigman, D. M., Chen, M. T., & Kao, S. J.. Elevated foraminifera-bound nitrogen isotopic composition during the last ice age in the South China Sea and its global and regional implications. Global Biogeochemical Cycles, 26(1) (2012).

https://doi.org/10.5194/egusphere-2025-1182
Preprint. Discussion started: 25 March 2025

109. Reimer, P. J., Austin, W. E., Bard, E., Bayliss, A., Blackwell, P. G., Ramsey, C. B., ... & Talamo, S. The IntCal20 Northern Hemisphere radiocarbon age calibration curve (0–55 cal kBP). Radiocarbon, 62(4), 725-757 (2020).
110. Riechelson, H., Rosenthal, Y., Bova, S., & Robinson, R. S. Southern Ocean biological pump role in driving Holocene atmospheric CO_2: Reappraisal. Geophysical Research Letters, 51(4), e2023GL105569 (2024).
111. Risgaard-Petersen, N. et al. Evidence for complete denitrification in a benthic foraminifer. Nature 443, 93–96 (2006).
112. Robinson, R. S., Martinez, P., Pena, L. D., & Cacho, I. Nitrogen isotopic evidence for deglacial changes in nutrient supply in the eastern equatorial Pacific. Paleoceanography, 24(4) (2009).
113. Robinson, R. S., Mix, A., & Martinez, P. Southern Ocean control on the extent of denitrification in the southeast Pacific over the last 70 ka. Quaternary Science Reviews, 26(1-2), 201-212 (2007).
114. Robinson, R. S., Sigman, D. M., DiFiore, P. J., Rohde, M. M., Mashiotta, T. A., & Lea, D. W. Diatom-bound 15N/14N: New support for enhanced nutrient consumption in the ice age subantarctic. Paleoceanography, 20(3) (2005).
115. Romanova, V., Lohmann, G., Grosfeld, K., & Butzin, M. The relative role of oceanic heat transport and orography on glacial climate. Quaternary science reviews, 25(7-8), 832-845 (2006).
116. RStudio Team. RStudio: Integrated Development for R. RStudio, Inc., Boston, MA (2023).
117. Russell, J. L., & Dickson, A. G. Variability in oxygen and nutrients in South Pacific Antarctic intermediate water. Global biogeochemical cycles, 17(2) (2003).
118. Salvatteci, R., Gutiérrez, D., Field, D., Sifeddine, A., Ortlieb, L., Bouloubassi, I., ... & Cetin, F. The response of the Peruvian Upwelling Ecosystem to centennial-scale global change during the last two millennia. Climate of the Past, 10(2), 715-731 (2014).
119. Salvatteci, R., Gutiérrez, D., Sifeddine, A., Ortlieb, L., Druffel, E., Boussafir, M., & Schneider, R. Centennial to millennial-scale changes in oxygenation and productivity in the Eastern Tropical South Pacific during the last 25,000 years. Quaternary Science Reviews, 131, 102-117 (2016).
120. Salvatteci, R., Schneider, R. R., Blanz, T., & Mollier-Vogel, E.. Deglacial to Holocene ocean temperatures in the Humboldt Current System as indicated by alkenone paleothermometry. Geophysical Research Letters, 46(1), 281-292 (2019).
121. Schlitzer, Reiner, Ocean Data View, odv.awi.de, 2023.
122. Schmidtko, S., Stramma, L. & Visbeck, M. Decline in global oceanic oxygen content during the past five decades. Nature 542, 335–339 (2017).
123. Scholz, F., McManus, J., Mix, A. C., Hensen, C., & Schneider, R. R.. The impact of ocean deoxygenation on iron release from continental margin sediments. *Nature Geoscience*, *7*(6), 433-437 (2014).
124. Scholz, F., Schmidt, M., Hensen, C., Eroglu, S., Geilert, S., Gutjahr, M., & Liebetrau, V. Shelf-to-basin iron shuttle in the Guaymas Basin, Gulf of California. Geochimica et Cosmochimica Acta, 261, 76-92 (2019).
125. Schubert, C. J., & Calvert, S. E. Nitrogen and carbon isotopic composition of marine and terrestrial organic matter in Arctic Ocean sediments: implications for nutrient utilization and organic matter composition. Deep Sea Research Part I: Oceanographic Research Papers, 48(3), 789-810 (2001).

https://doi.org/10.5194/egusphere-2025-1182
Preprint. Discussion started: 25 March 2025

126. Seki, O., Ikehara, M., Kawamura, K., Nakatsuka, T., Ohnishi, K., Wakatsuchi, M., ... & Sakamoto, T. Reconstruction of paleoproductivity in the Sea of Okhotsk over the last 30 kyr. Paleoceanography, 19(1) (2004).
127. Sigman, D. M., Altabet, M. A., Michener, R., McCorkle, D. C., Fry, B., & Holmes, R. M. Natural abundance-level measurement of the nitrogen isotopic composition of oceanic nitrate: an adaptation of the ammonia diffusion method. Marine chemistry, 57(3-4), 227-242 (1997).
128. Skinner, L. C., Fallon, S., Waelbroeck, C., Michel, E., & Barker, S. Ventilation of the deep Southern Ocean and deglacial CO2 rise. Science, 328(5982), 1147-1151 (2010).
129. Somes, C. J., Schmittner, A., Muglia, J., & Oschlies, A. A three-dimensional model of the marine nitrogen cycle during the last glacial maximum constrained by sedimentary isotopes. Frontiers in Marine Science, 4, 108 (2017).
130. Stramma, L., Johnson, G. C., Sprintall, J. & Mohrholz, V. Expanding oxygen-minimum zones in the tropical oceans. Science 320(5876), 655–658 (2008).
131. Stramma, L., Schmidtko, S., Levin, L. A. & Johnson, G. C. Ocean oxygen minima expansions and their biological impacts. Deep-Sea Res. I Ocean. Res. Pap. 57(4), 587–595 (2010).
132. Studer, A. S., Mekik, F., Ren, H., Hain, M. P., Oleynik, S., Martínez-García, A., ... & Sigman, D. M.. Ice age-Holocene similarity of foraminifera-bound nitrogen isotope ratios in the eastern equatorial Pacific. Paleoceanography and Paleoclimatology, 36(5), e2020PA004063 (2021).
133. Takano, Y., Ito, T., & Deutsch, C. Projected centennial oxygen trends and their attribution to distinct ocean climate forcings. Global Biogeochemical Cycles, 32(9), 1329-1349 (2018).
134. Taylor, M. A., Hendy, I. L., & Chappaz, A. Assessing oxygen depletion in the Northeastern Pacific Ocean during the last deglaciation using I/Ca ratios from multiple benthic foraminiferal species. Paleoceanography, 32(8), 746-762 (2017).
135. Ternois, Y., Kawamura, K., Keigwin, L., Ohkouchi, N., & Nakatsuka, T. A biomarker approach for assessing marine and terrigenous inputs to the sediments of Sea of Okhotsk for the last 27,000 years. Geochimica et Cosmochimica Acta, 65(5), 791-802 (2001).
136. Tesdal, J. E., Galbraith, E. D., & Kienast, M. (2013). Nitrogen isotopes in bulk marine sediment: linking seafloor observations with subseafloor records. *Biogeosciences*, *10*(1), 101-118.
137. Thunell, R. C., Sigman, D. M., Muller-Karger, F., Astor, Y., & Varela, R. Nitrogen isotope dynamics of the Cariaco Basin, Venezuela. Global Biogeochemical Cycles, 18(3) (2004).
138. Ujiié, H., & Ujiié, Y. Late Quaternary course changes of the Kuroshio Current in the Ryukyu Arc region, northwestern Pacific Ocean. Marine Micropaleontology, 37(1), 23-40 (1999).
139. Van Geen, A., Fairbanks, R. G., Dartnell, P., McGann, M., Gardner, J. V., & Kashgarian, M. Ventilation changes in the northeast Pacific during the last deglaciation. Paleoceanography, 11(5), 519-528 (1996).
140. Voss, M. et al. The marine nitrogen cycle: Recent discoveries, uncertainties and the potential relevance of climate change. Philos. Trans. R. Soc. B Biol. Sci. 368, 293–296 (2013).
141. Wada, E., and Hattori, A. Nitrogen isotope effects in the assimilation of inorganic nitrogenous compounds by marine diatoms. Geomicrobiol. J. 1, 85–101 (1978).
142. Waelbroeck, C., Frank, N., Jouzel, J., Parrenin, F., Masson-Delmotte, V., & Genty, D. Transferring radiometric dating of the last interglacial sea level high stand to marine and ice core records. Earth and Planetary Science Letters, 265(1-2), 183-194 (2008).

https://doi.org/10.5194/egusphere-2025-1182
Preprint. Discussion started: 25 March 2025

143. Wallmann, K., Schneider, B. & Sarntheim, M. Effects of eustatic sea-level change, ocean dynamics, and nutrient utilization on atmospheric pCO2 and seawater composition over the last 130 000 years: a model study. Clim. Past.12, 339–375 (2016).
144. Wallmann, K., José, Y. S., Hopwood, M. J., Somes, C. J., Dale, A. W., Scholz, F., ... & Oschlies, A. Biogeochemical feedbacks may amplify ongoing and future ocean deoxygenation: a case study from the Peruvian oxygen minimum zone. Biogeochemistry, 159(1), 45-67 (2022).
145. Wang, Y., Hendy, I. L., & Thunell, R. Local and remote forcing of denitrification in the northeast Pacific for the last 2,000 years. Paleoceanography and Paleoclimatology, 34(8), 1517-1533 (2019).
146. Wang, Y., Hendy, I. L., & Zhu, J. Expansion of the Southern California oxygen minimum zone during the early-to mid-Holocene due to reduced ventilation of the Northeast Pacific. Quaternary Science Reviews, 238, 106326 (2020).
147. White, A. E., Foster, R. A., Benitez-Nelson, C. R., Masqué, P., Verdeny, E., Popp, B. N., ... & Prahl, F. G. Nitrogen fixation in the Gulf of California and the eastern tropical North Pacific. Progress in Oceanography, 109, 1-17 (2013).
148. Woehle, C. et al. A Novel Eukaryotic Denitrification Pathway in Foraminifera. Curr. Biol. 28, 2536-2543.e5 (2018).
149. Woehle, C. et al. Denitrification in foraminifera has an ancient origin and is complemented by associated bacteria. Proc. Natl. Acad. Sci. U. S. A. 119, (2022).
150. Yamamoto, A., Abe-Ouchi, A., Shigemitsu, M., Oka, A., Takahashi, K., Ohgaito, R., & Yamanaka, Y. Global deep ocean oxygenation by enhanced ventilation in the Southern Ocean under long-term global warming. Global Biogeochemical Cycles, 29(10), 1801-1815 (2015).